SANDIA REPORT

SAND2014-19350
Unlimited Release
Printed October and 2014

Infrasound Generation from the HH Seismic Hammer

Kyle R. Jones

Prepared by
Sandia National Laboratories
Albuquerque, New Mexico 87185 and Livermore, California 94550

Sandia National Laboratories is a multi-program laboratory managed and operated by Sandia Corporation, a wholly owned subsidiary of Lockheed Martin Corporation, for the U.S. Department of Energy's National Nuclear Security Administration under contract DE-AC04-94AL85000.

Issued by Sandia National Laboratories, operated for the United States Department of Energy by Sandia Corporation.

Available to DOE and DOE contractors from
U.S. Department of Energy
Office of Scientific and Technical Information
P.O. Box 62
Oak Ridge, TN 37831

Telephone: (865) 576-2087
Facsimile: (865) 576-5728
E-Mail: reports@adonis.osti.gov
Online ordering: http://www.osti.gov/bridge

Available to the public from
U.S. Department of Commerce
National Technical Information Service
5301 Shawnee Rd
Alexandria, VA 22312

Telephone: (800) 553-6847
Facsimile: (703) 605-6900
E-Mail: orders@ntis.gov
Online order: http://www.ntis.gov/help/ordermethods.aspx#online

SAND2014-19350
Unlimited Release
Printed October 2014

Infrasound Generation from the HH Seismic Hammer

Kyle R. Jones
Department Names
Sandia National Laboratories
P.O. Box 5800
Albuquerque, New Mexico 87185-MS404

Abstract

The HH Seismic hammer is a large, "weight-drop" source for active source seismic experiments. This system provides a repetitive source that can be stacked for subsurface imaging and exploration studies. Although the seismic hammer was designed for seismological studies it was surmised that it might produce energy in the infrasonic frequency range due to the ground motion generated by the 13 metric ton drop mass. This study demonstrates that the seismic hammer generates a consistent acoustic source that could be used for in-situ sensor characterization, array evaluation and surface-air coupling studies for source characterization.

ACKNOWLEDGMENTS

We would like to acknowledge Bob White of National Securities Technologies for providing invaluable field assistance, support and supplies, without which this project could not have happened on such short notice. We would also like to thank Stephen Arrowsmith from Los Alamos National Laboratory for loaning us equipment. Finally, thanks to John Hampshire of HH Seismic for the opportunity to observe and record the hammer.

CONTENTS

FIGURES

TABLES

NOMENCLATURE

DOE	Department of Energy
SH	Seismic Hammer
SPE	Source Physics Experiment
NSTec	National Security Technolgoies
SNL	Sandia National Laboratories

1. INTRODUCTION

The HH Seismic Hammer (SH) has been developed to generate large, repetitive sources for active source seismic experiments. Researchers with the Source Physics Experiment (SPE) are currently planning to use the SH at the Nevada National Security Site for an active source experiment to compliment the SPE underground explosions. As a part of the project the SH has been deployed at a crane yard in North Las Vegas for testing, evaluation and demonstration. During the last demonstration event we were invited to deploy infrasound sensors around the crane yard to determine if the SH produced energy in the infrasonic range (<20 Hz).

1.1. HH Seismic Hammer

According to documentation provided by HH Seismic the SH (Fig. 1) is an impulsive source capable of generating up to .19 megajoules of energy by hydraulically lifting and then dropping a 13 metric ton mass from a height of 1.5 m. The hammer is capable of up to 3 shots per minute with remarkable consistency.

Figure 1. The HH Seismic Hammer deployed during the experiment.

1.2. Experiment Design

We deployed six seismically decoupled Hyperion Technology Group IFS-5 series infrasound sensors along with five Reftek digitizers. Figure 2 shows the deployment configuration for the experiment and Table 1 shows the exact locations of each sensor. Stations 1, 2, 5 and 6 operated correctly during the experiment while the Reftek recording sensors 3 and 4 malfunctioned and recorded only noise. The digitizers were configured to record at 1000 Hz with a gain of 32.

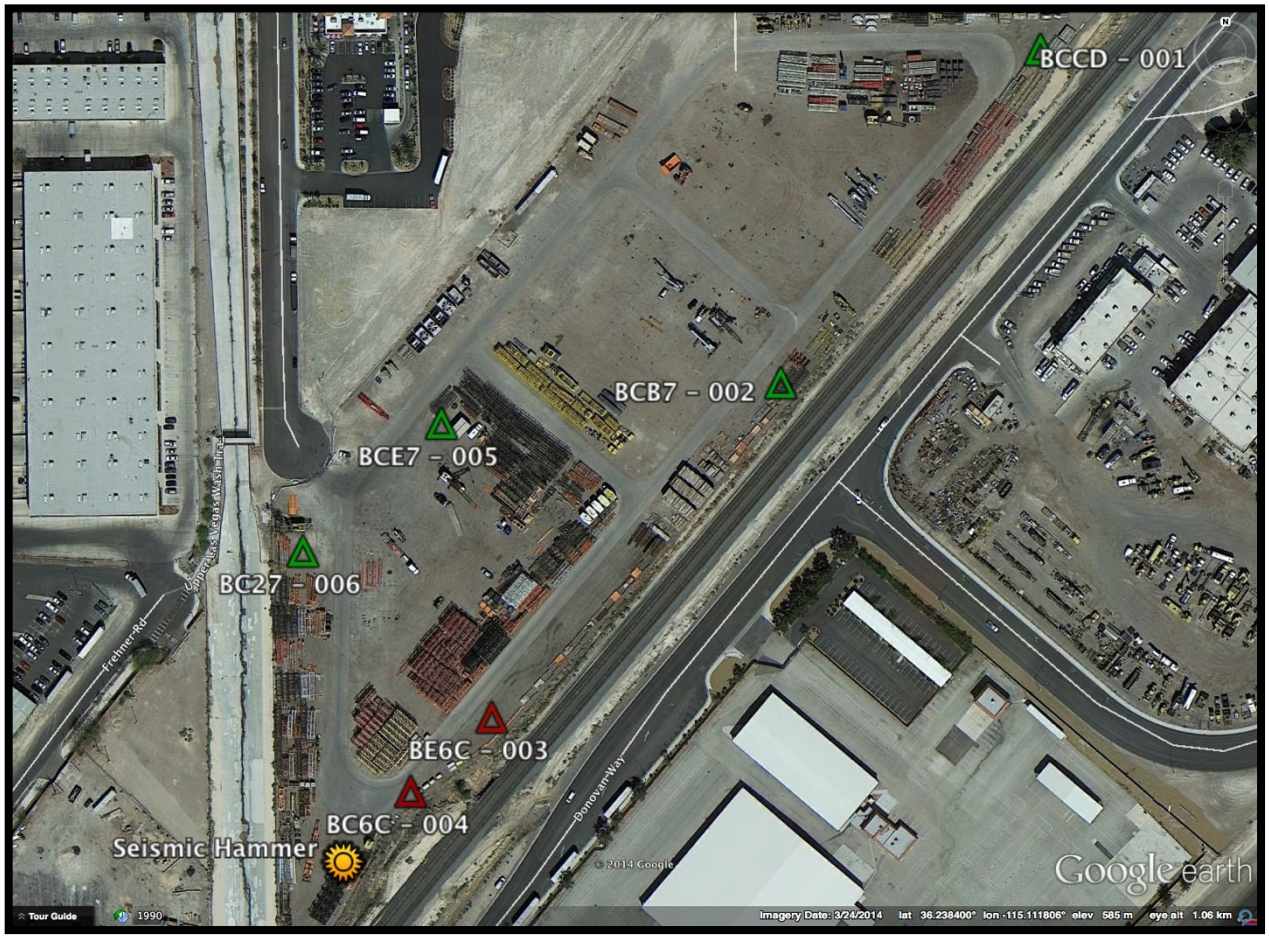

Figure 2. Map showing the North Las Vegas crane yard and deployment configuration of the sensors. The SH was located to the southwest and the triangles show the locations of the infrasound sensors. Green triangles represent the working sensors and the red represent malfunctioning equipment. The distance from the SH to the farthest station (BCCD) is ~460 m.

Table 1. Location and configuration table of each site.

Station	Latitude	Longitude	Elevation (m)	Distance to SH (m)
1 - BCCD	36.239541888	-115.108161295	586.16	460
2 - BCB7	36.238242465	-115.109415691	585.06	275
3 - BE6C	36.236932040	-115.110819756	583.50	85
4 - BE6C	36.236641017	-115.111213905	581.58	35
5 - BEC7	36.238083979	-115.111063745	584.50	188
6 - BC27	36.237583380	-115.111736644	583.59	130

2. DATA PROCESSING

Data were collected between the hours of 10:00 and 12:00 UTC (3:00 and 5:00 am PDT). The experiment was conducted in the early morning to ensure the low-noise conditions were optimal for infrasound propagation. Surface winds were negligible and the temperature was 77 degrees Fahrenheit. The data were collected and converted from the raw Reftek format to SAC format for processing (Fig. 3).

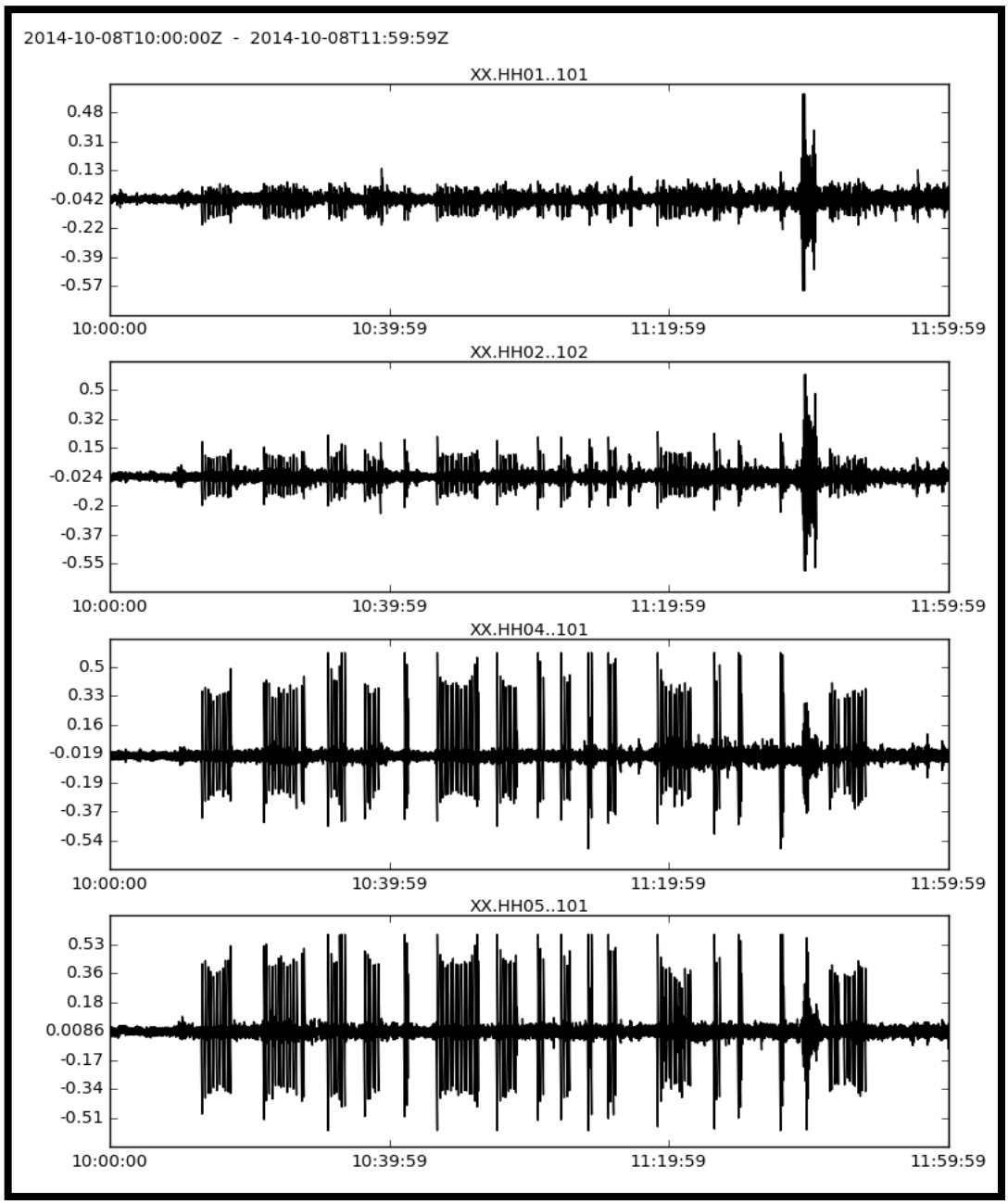

Figure 3. Unfiltered waveforms from stations 1, 2, 5 and 6 (top to bottom). The large event near 11:40 UTC was a passing train while all of the other "spikes" are from the hammer. Amplitude is in Pa.

2.1. Event Detection

In order to extract each shot in an efficient manner we used the ObsPy "zDetect" function (Fig. 4), which is based on a seismic event detection algorithm called the Z-Statistic (Withers et al., 1998). We used the closest station (6) to maximize event detection and minimize false triggers. For a complete trigger table see Appendix C.

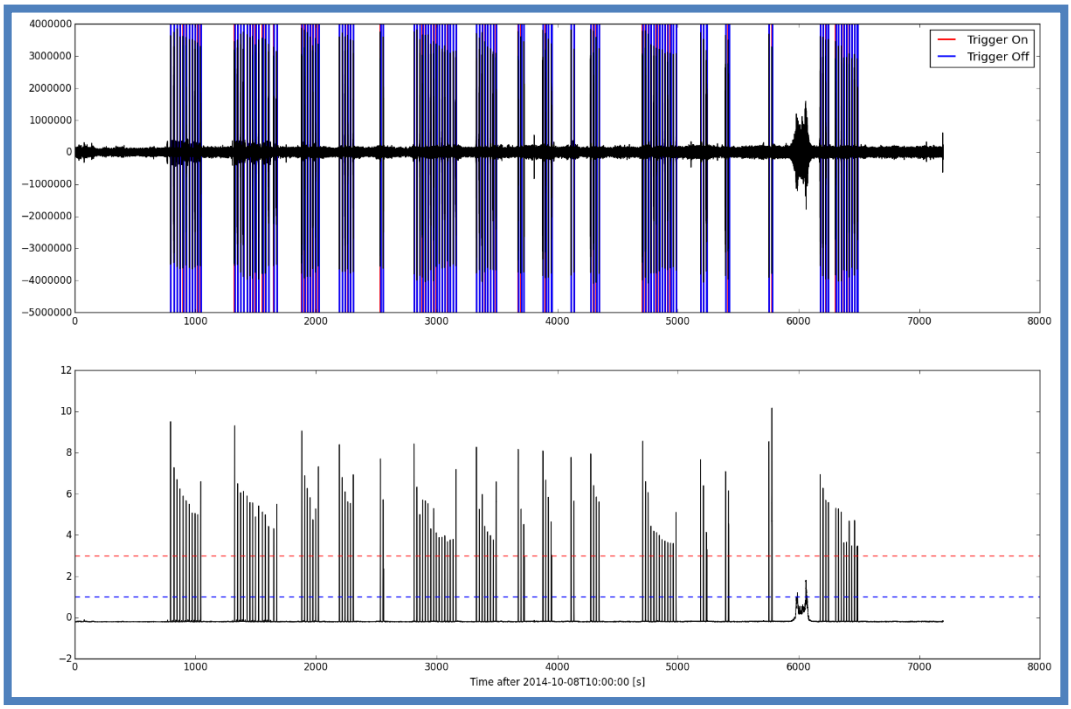

Figure 4. Plot showing the results of the zDetect function. The top panel shows all of the events that the algorithm triggered on. The bottom panel shows the triggers and corresponding thresholds. Note that the train did not trigger.

2.2. Signal Analysis

The generated trigger list was parsed and each event windowed across the network. A brief analysis was conducted to determine where the dominant energy was prior to further data processing. Figure 5 shows an example spectrogram from one of the triggered events. The dominant energy is centered around 10 Hz with a secondary peak centered at 95 Hz. The secondary peak is technically in the acoustic range as it is above 20 Hz.

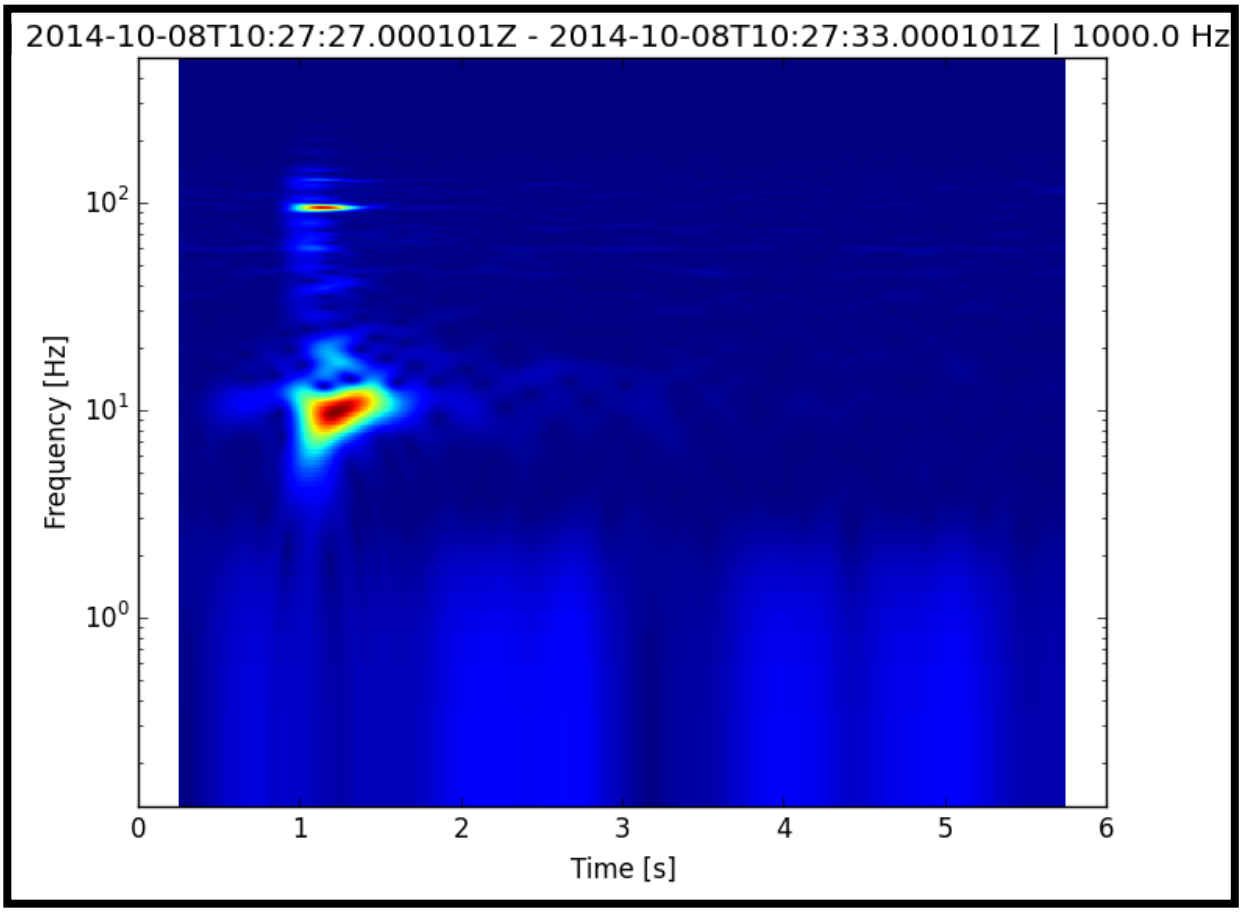

Figure 5. Spectrogram from one of the triggered events. Peaks occur at 10 Hz and 95 Hz with the latter occurring above the range of infrasound (> 20 Hz).

During testing it was noticed that occasionally there was a secondary pulse after the primary shot much like if the weight "bounced" after the initial shot (Fig. 6). Of note is that even this secondary pulse had remarkably similar energy content to the primary shot (both infrasonic and acoustic) and is nearly identical visually in the time domain.

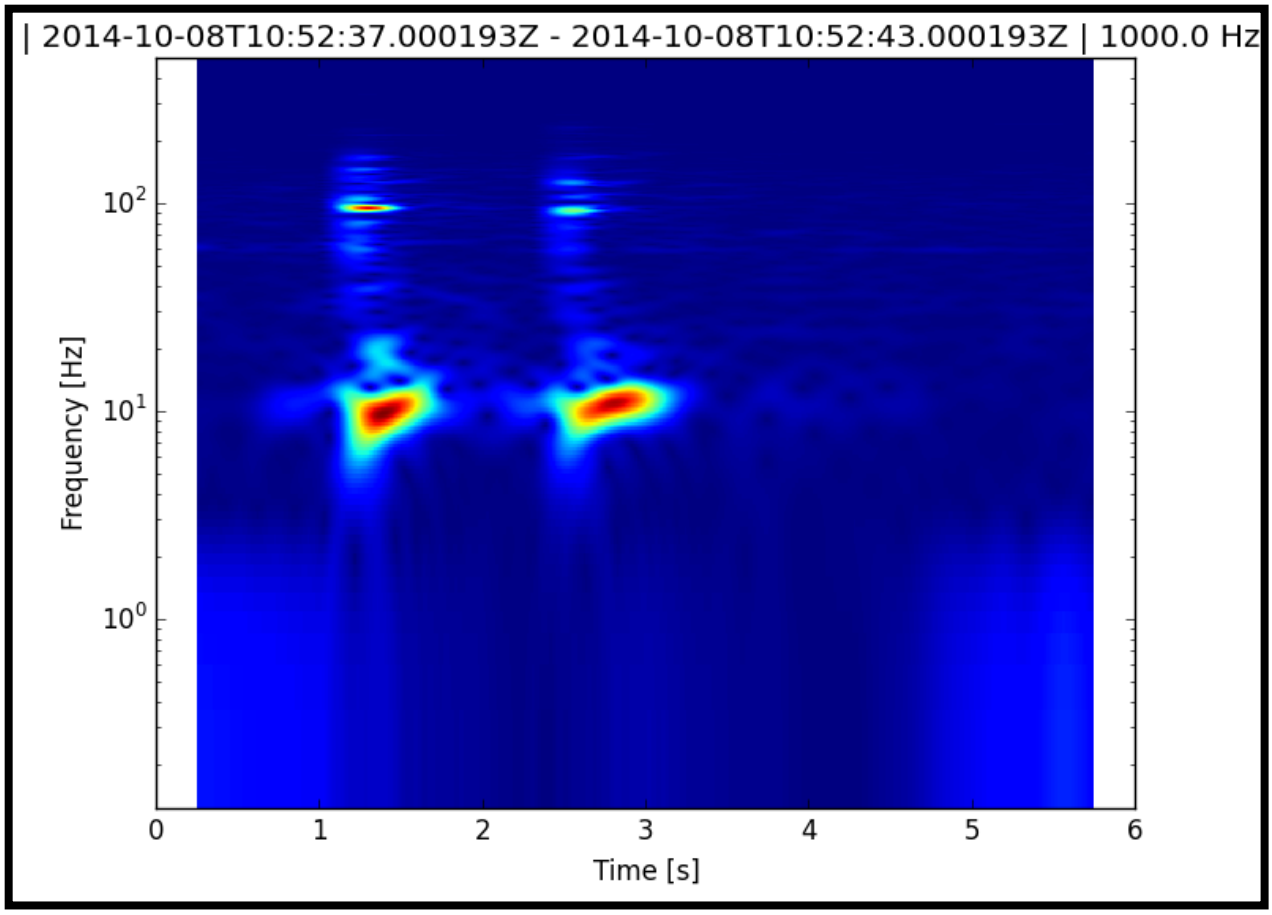

Figure 6. Spectrogram showing a "double" pulse. From visual observation, the hammer occasionally bounced after the initial shot. Note that even this secondary pulse produces similar energy as the primary pulse.

Figure 7 shows what the time series looks like when filtered between 5 – 15 Hz and 80 – 110 Hz. When filtered in the lower frequency range the hammer shots are accentuated while the train signal is reduced and when filtered in the higher range the opposite is true. The amplitudes of the events were not very large (0.5 Pa max) and quickly decayed at a rate of 1/r from the source. At the farthest station the amplitude was less than 0.1 Pa.

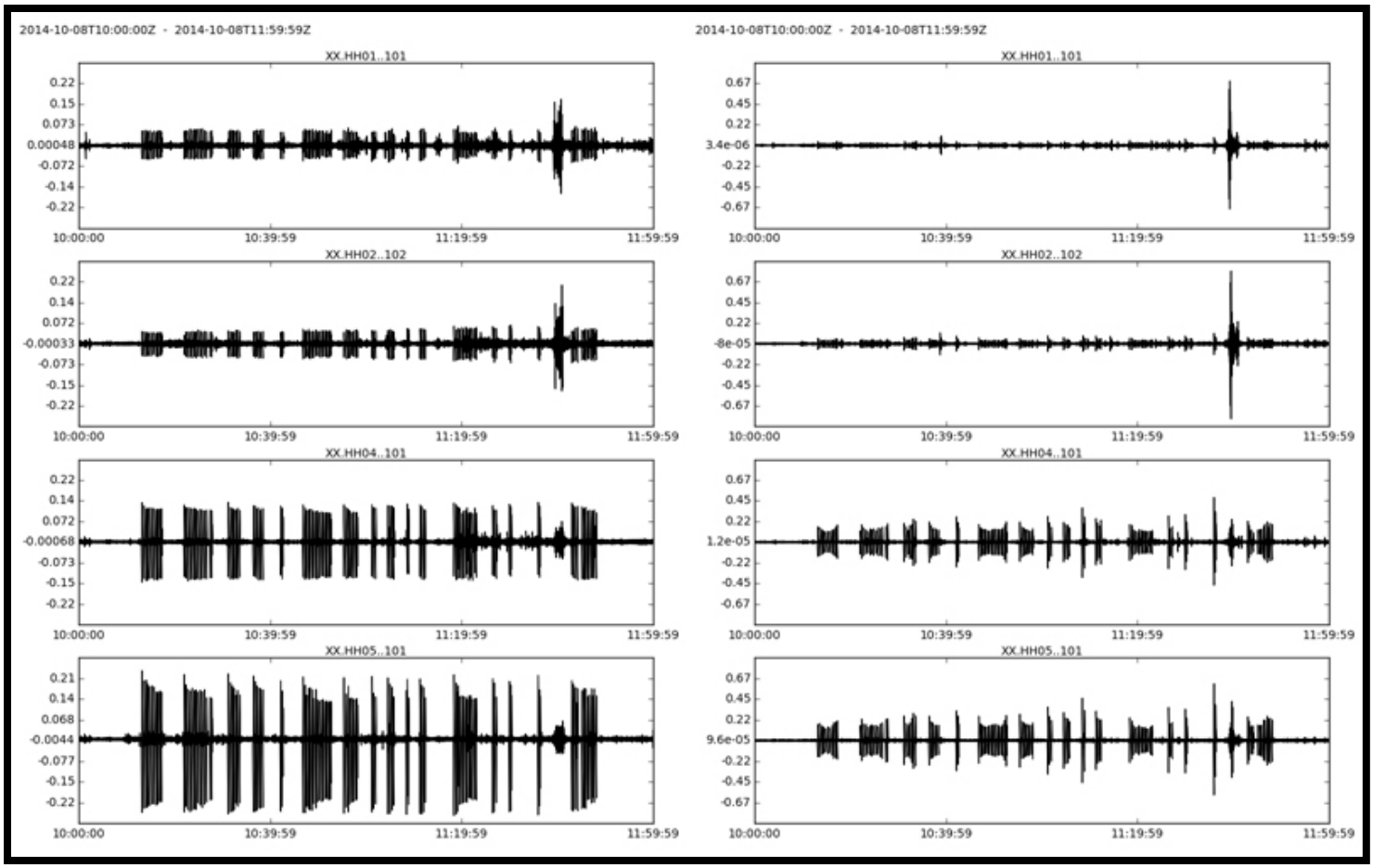

Figure 7. Waveform plots filtered around both peaks 5-15 Hz (left) and 80-110 Hz (right). Note that the low frequency energy (infrasound) on the left is accentuated while the filter on the right brings out the more audible frequencies such as the train. Amplitude is in Pa.

2.2. Source Inversion

Infrasound event processing traditionally utilizes two techniques for source localization. Infrasound arrays are used for signal detection and location of events that originate from longer distances. These data are processed using FK analysis and back-azimuths are calculated. When enough arrays detect the event the back-azimuths are mapped to their crossing points and a location is generated. The other technique is network processing using grid search or source inversion and can be done with a network of single sensors. For the SH experiment we were constrained both in physical space and available equipment and thus opted for the network source inversion technique.

The inversion technique that we used is based on the earthquake location inverse problem described by Stein and Wysession, 2003 where acoustic sources are located by iteratively solving for the source position in the x and y directions while minimizing the residual error after each iteration. It uses a simple time of arrival matrix that is seeded with acoustic sound speed, elevation and the mean latitude and longitude of the sensor network.

The data are windowed, filtered and cross-correlated with respect to station 6 (the closest station). The cross correlation gives us the time lag between station 6 (0 second lag) and the

other three stations (+/- x second lag). The time lags for each event are relative to station 6 and can be found in Appendix C. We noted the temperature during the experiment to be 77 degrees Fahrenheit corresponding to a sound speed of 346 m/s. For the inversion we fixed the sound speed and elevation because the temperature did not vary and the elevation of the hammer was known. This makes the inversion simple as we are only solving for x and y.

The source inversion worked best when using signals that were broadband filtered between 5 and 110 Hz. The reason for this is that when narrow band filtering around the lower frequencies there is a certain amount of "ringing" in the waveform (Fig. 8 left panel) that makes it difficult for the cross-correlation algorithm to accurately line up the signals. This resulted in many mislocated events. When we included some of the higher frequencies a more impulsive signal emerged (Fig. 8 right panel), resulting in better cross-correlation alignment and subsequently better source locations with fewer mislocations.

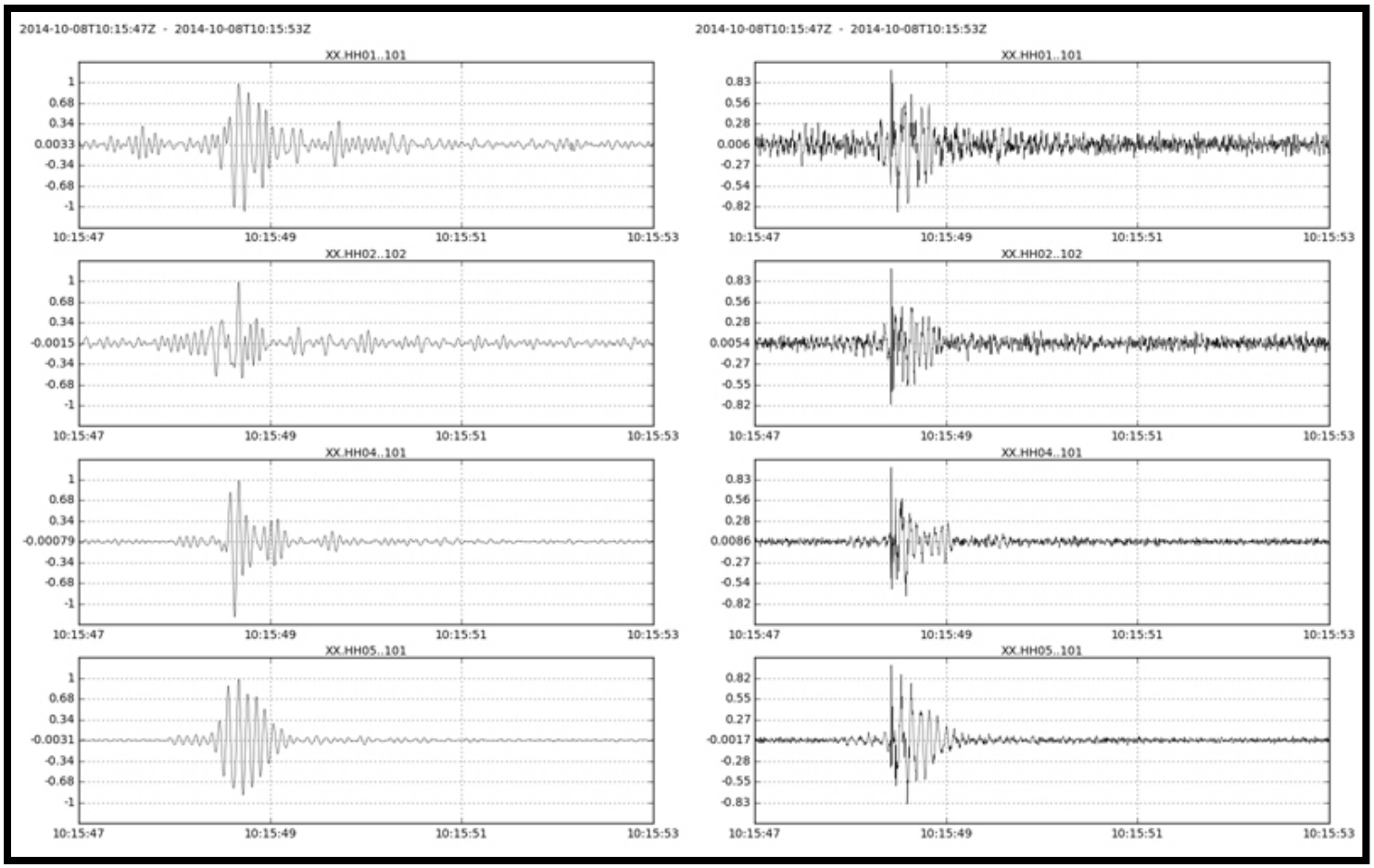

Figure 8. Example of aligned waveforms used in the inversion filtered between 5 – 15 Hz (left) and 5 – 110 Hz (right). The waveforms filtered between 5 – 15 Hz produced more mislocated events than the more broadband filtered signal. Amplitude is in Pa.

The results of the source inversion agree well with the location of the SH (within ~10 m). Figure 9 shows the locations of each triggered event. The sources are constrained east/west to within 5

m and 20 m north/south. The drift north/south could be due to temperature changes over the duration of the experiment. Without a met station on site it would be difficult to determine that change accurately. The point of the source inversion was to conclude that the source was acoustic and not seismic (seismic energy propagating and shaking the sensor). To that end the variability is acceptable considering the locations are very close to the actual source. In future studies additional sensors azimuthally around the source and proper meteorological monitoring will better constrain the locations.

Figure 9. Source locations for all triggered events. Note that during the experiment the crates shown in the figure were not there. The locations are confined to 5 m east/west and 20 m north/south.

3. DISCUSSION AND CONCLUSIONS

We have demonstrated that the seismic hammer conclusively generates signal in both the infrasound (< 20 Hz) and acoustic (> 20 Hz) ranges. The SH is a remarkably consistent source that could be used for single sensor and array characterization, short-range source propagation studies and crustal source studies as proxies to underground chemical explosions for understanding the ground surface as a source. Furthermore, the SH could be used as an in-situ calibration and state of health source for IMS infrasound arrays.

With newer infrasound sensors increasing the range of detectible frequencies we are able to capture more information that would have traditionally been missed such as the SH generating two distinct frequency peaks in both the acoustic and infrasonic ranges. We are confident that the source of infrasound generation is the drop-weight and subsequent ground motion. However, the low frequency "ringing" observed in the signal should be better characterized and modeled. Although the SH clearly generates infrasound, it does so at relatively low amplitudes. With the closest station recording an amplitude of 0.5 Pa and the farthest < 0.1 Pa, the experiments need to be conducted in very quiet, low-noise conditions. This could prove challenging for future experiments in the field.

3.1. Future Work

The SH will be used in an active source characterization of portions of the Nevada National Security Site. We plan to install additional infrasound sensors azimuthally around the source during this field deployment. We hope to answer questions generated by the analysis of this first study. For example, do different surface geologies affect the amplitude or frequency of the hammer-generated infrasound? Does the hammer-generated infrasound propagate azimuthally in all directions or is there directivity to the source? Can we use hammer-generated infrasound studies to better understand the ground surface as an infrasound source and use that for discrimination of underground explosions after propagation through the atmosphere? Are there certain characteristics that are unique to different geologies that are observed in the infrasound waveform?

4. REFERENCES

1. Stein, S., and Wysession, M., *An Introduction to Seismology, Earthquakes and Earth Structure*, Blackwell Publishing Ltd.,2003, 497 pp., pg 415-424.

2. Withers, M., Aster, R., Young, C., Beiriger, J., Harris, M., Moore, S., Trujillo, J., *A comparison of select trigger algorithms for automated global seismic phase and event detection*, Bulletin of the Seismological Society of America, February 1998, 88(1):95-106.

APPENDIX A: WAVEFORM PLOTS

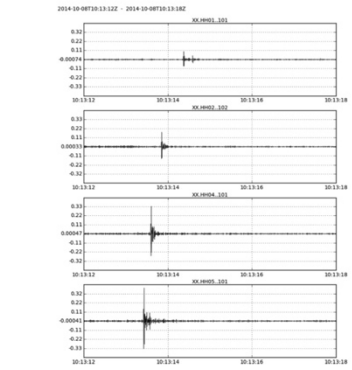

793.png

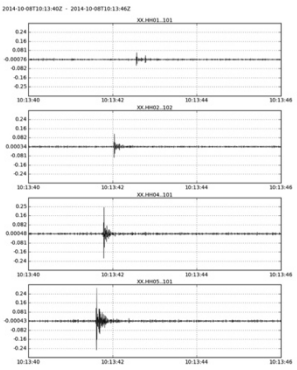

821.png

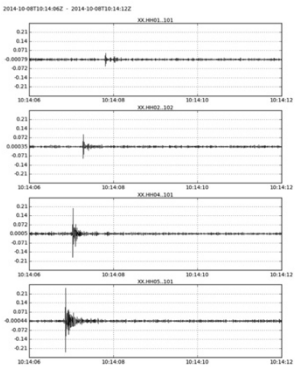

847.png

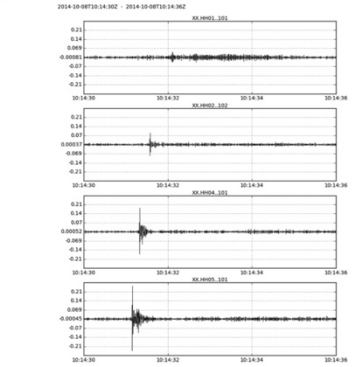

871.png

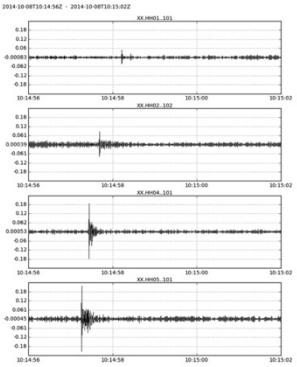

897.png

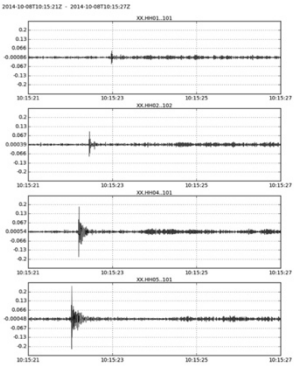

922.png

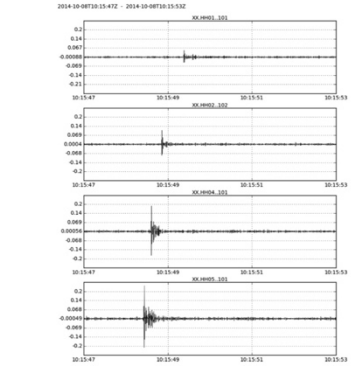

948.png

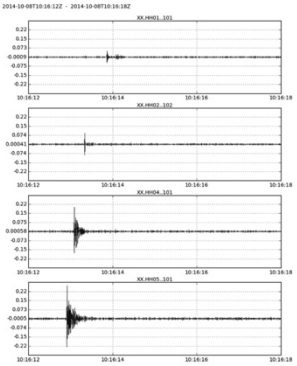

973.png

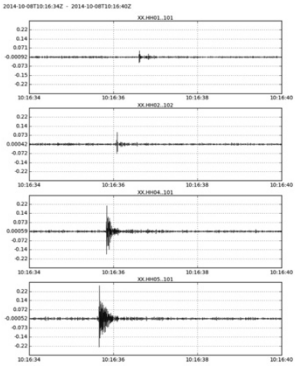

995.png

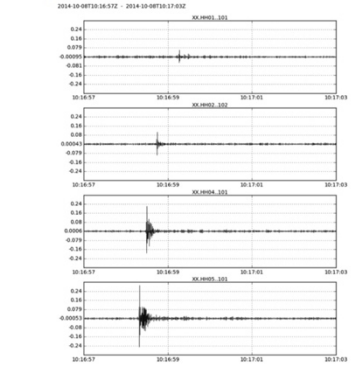

1018.png

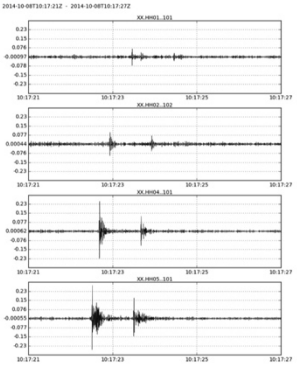

1042.png

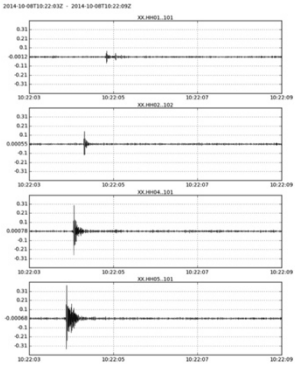

1324.png

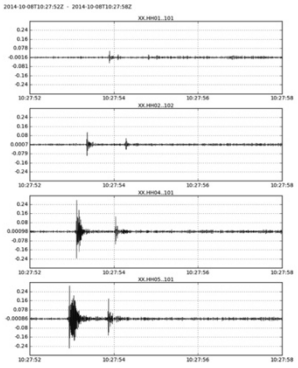

1673.png

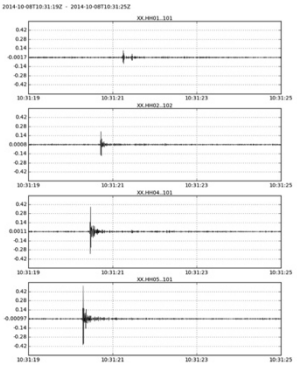

1880.png

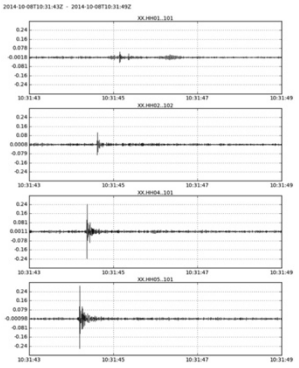

1904.png

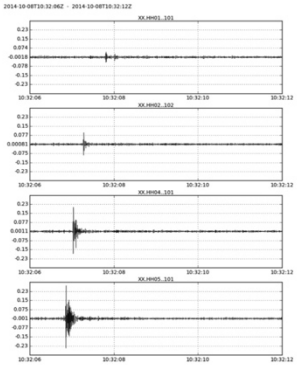

1927.png

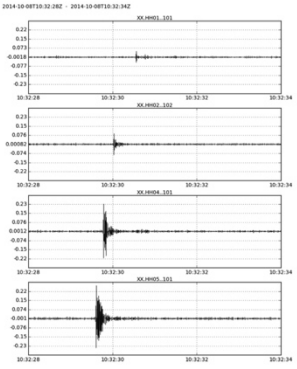

1949.png

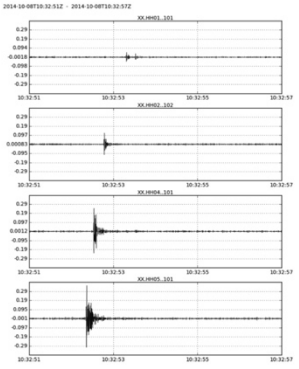

1972.png

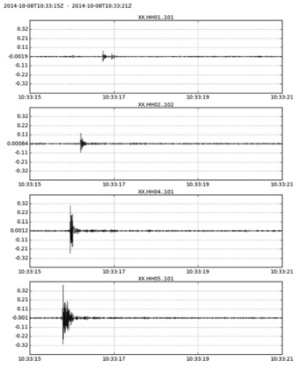

1996.png

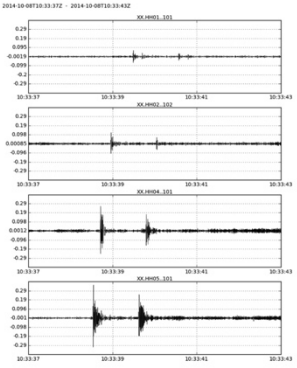

2018.png

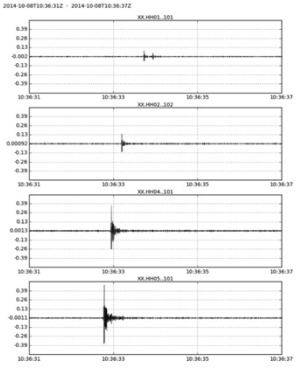

2192.png

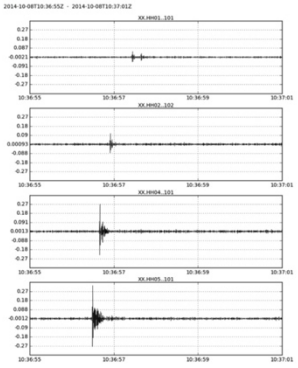

2216.png

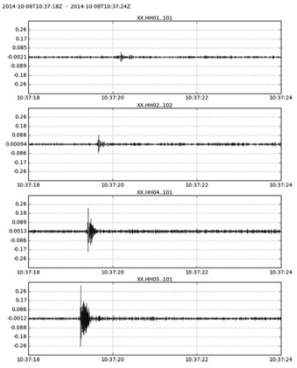

2239.png

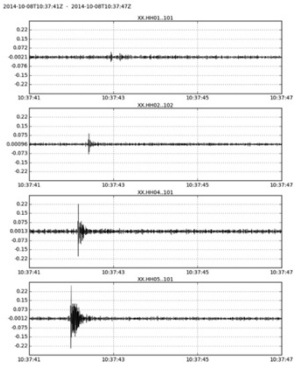

2262.png

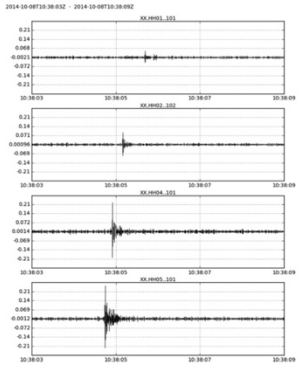

2284.png

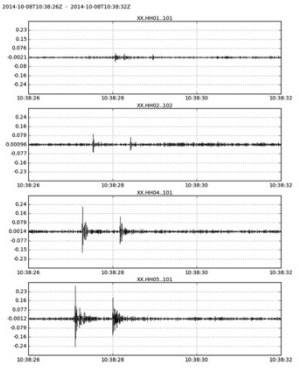

2307.png

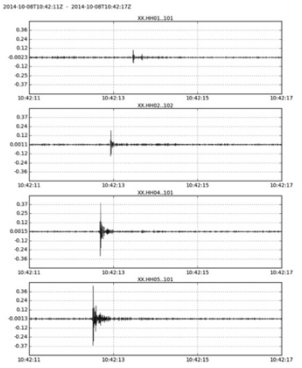

2532.png

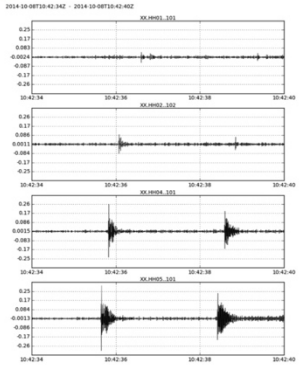

2555.png

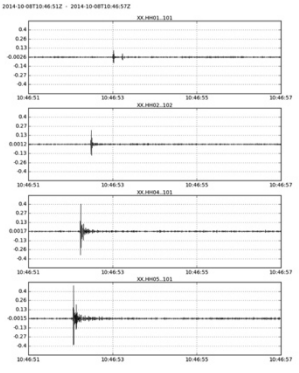

2812.png

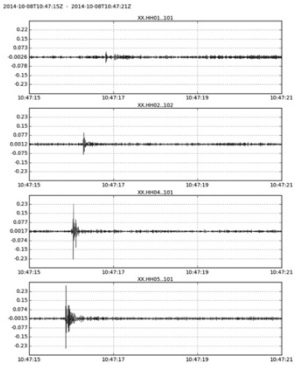

2836.png

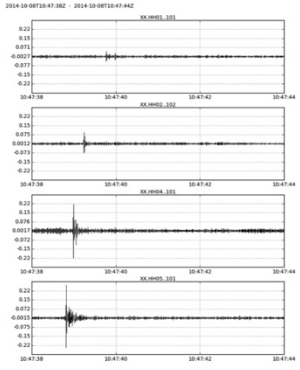

2859.png

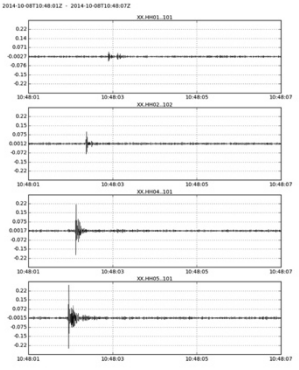

2882.png

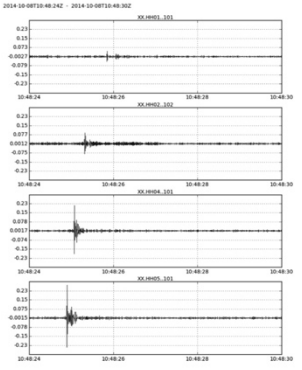

2905.png

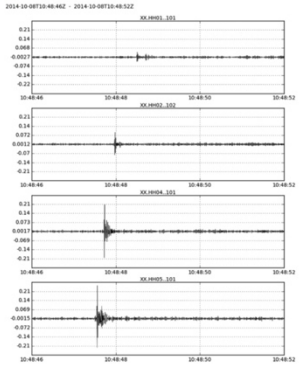

2927.png

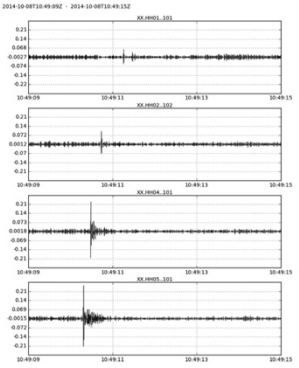

2950.png

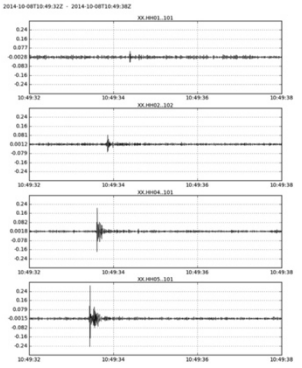

2973.png

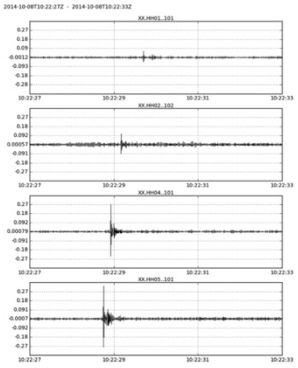

1348.png

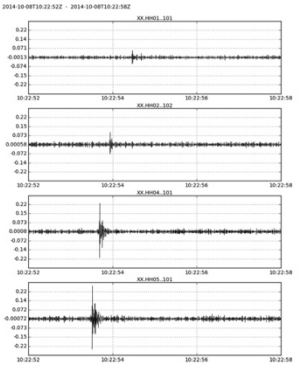

1373.png

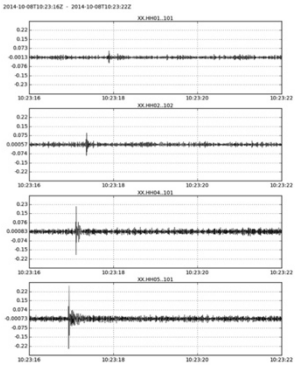

1397.png

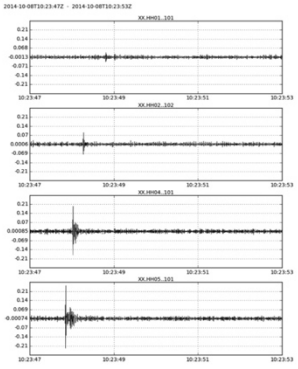

1428.png

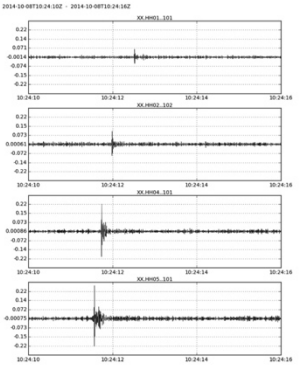

1451.png

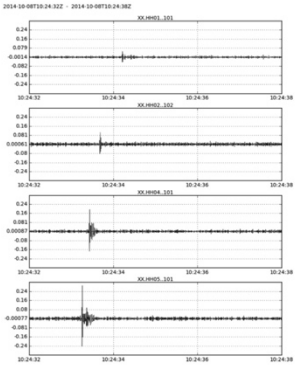

1473.png

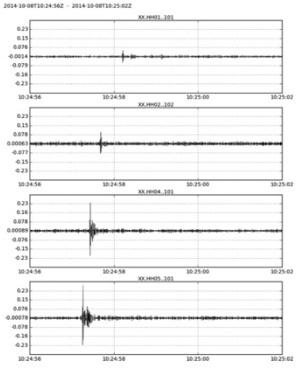

1497.png

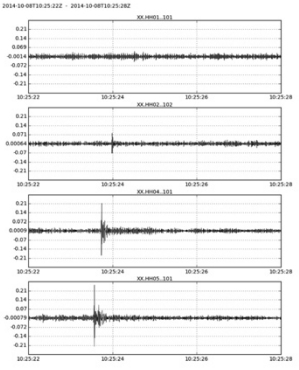

1523.png

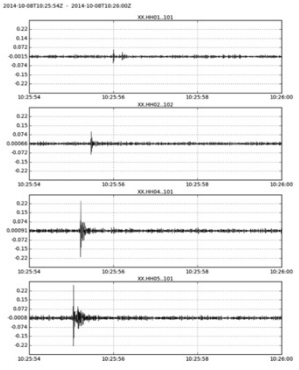

1555.png

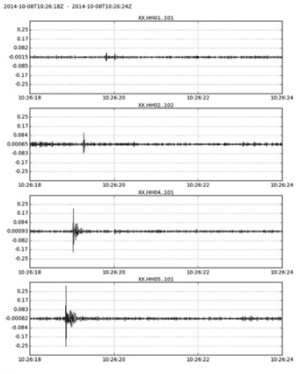

1579.png

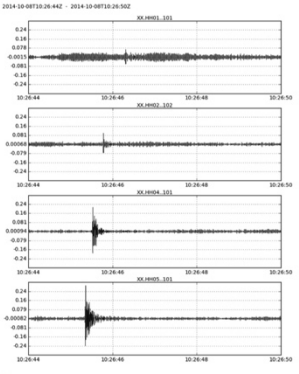

1605.png

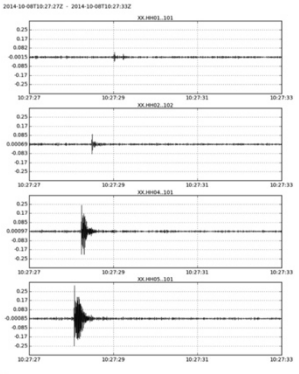

1648.png

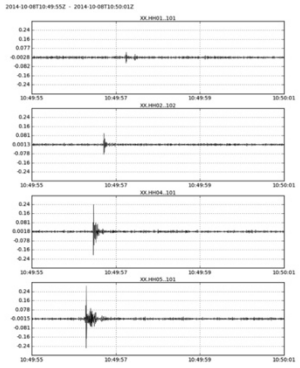

2996.png

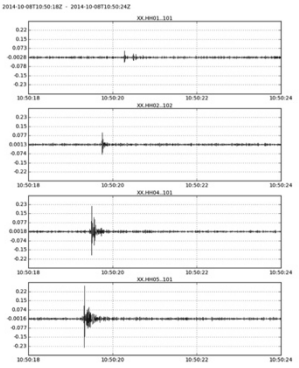

3019.png

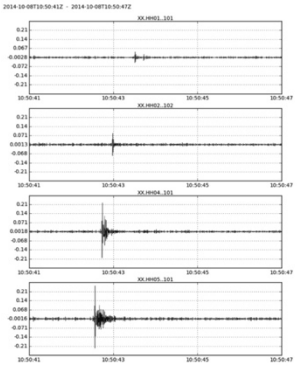

3042.png

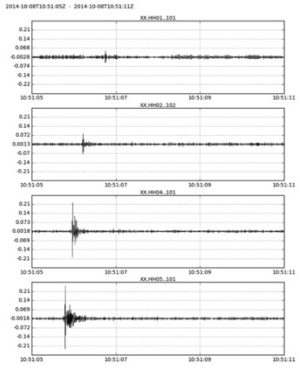

3066.png

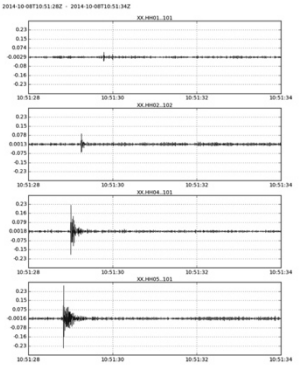

3089.png

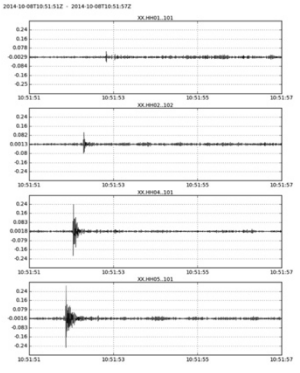

3112.png

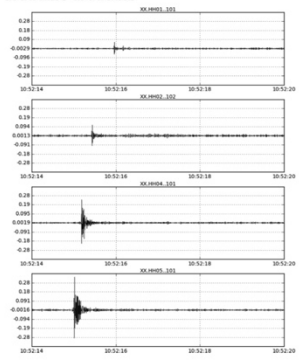

3135.png

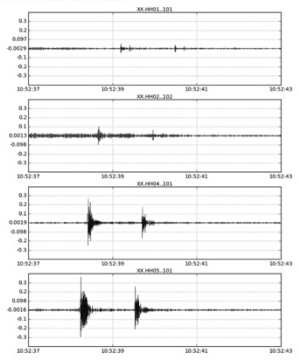

3158.png

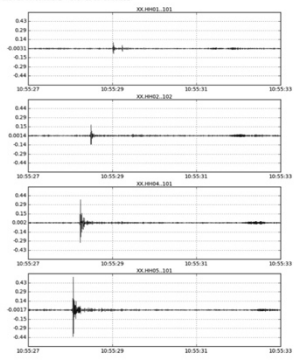

3328.png

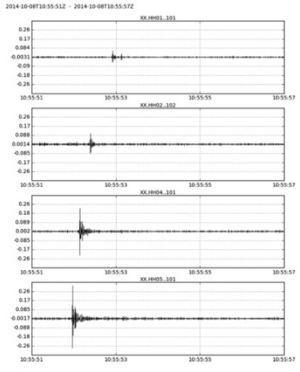

3352.png

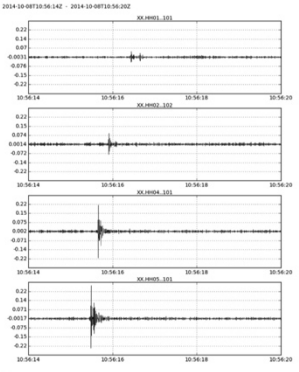

3375.png

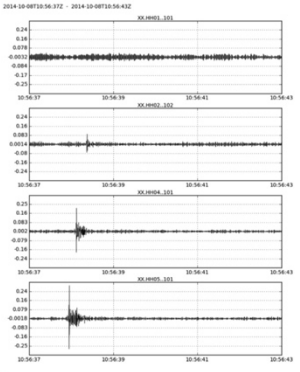

3398.png

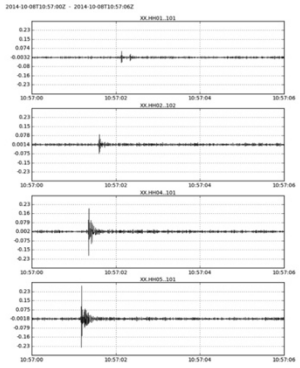

3421.png

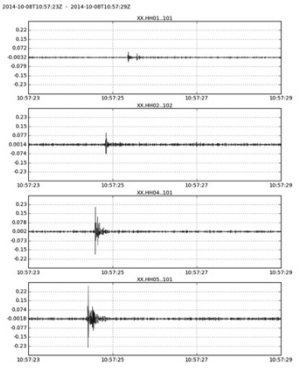

3444.png

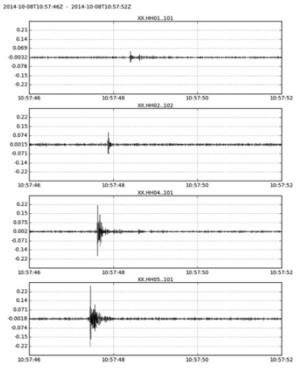

3467.png

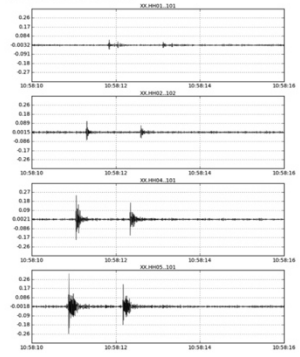

3491.png

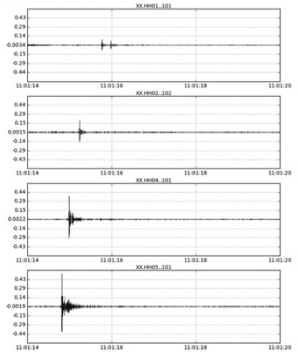

3675.png

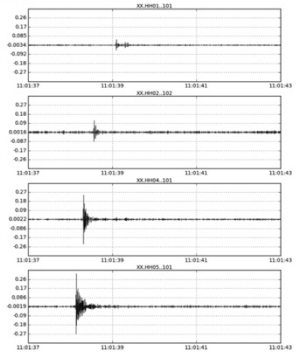

3698.png

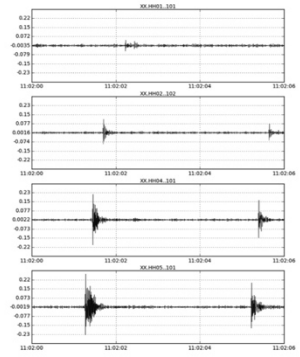

3721.png

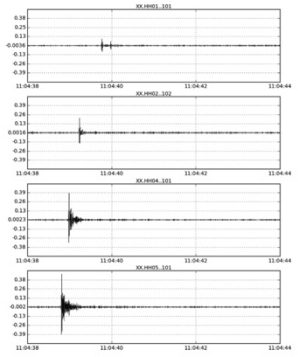

3879.png

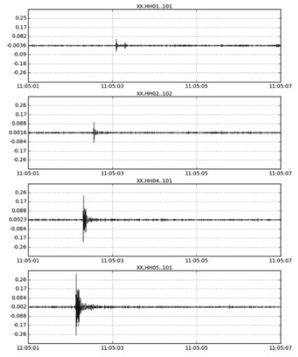

3902.png

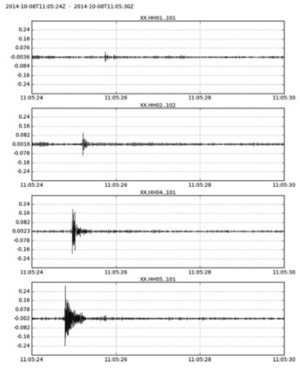

3925.png

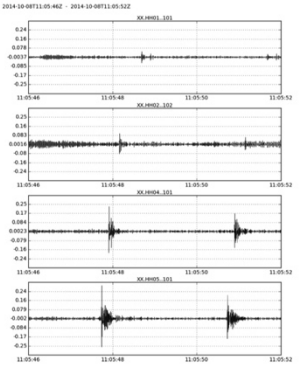

3947.png

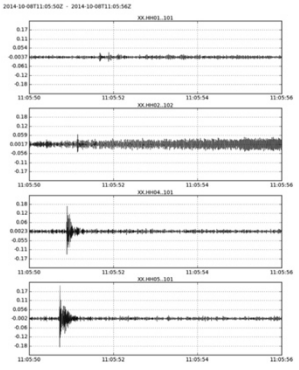

3951.png

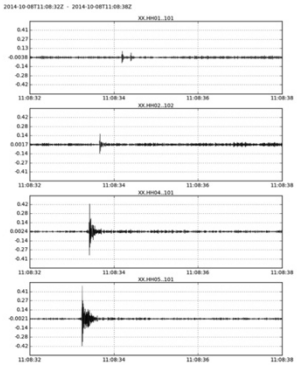

4113.png

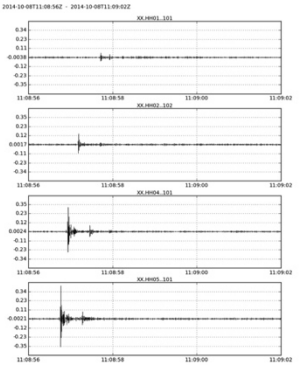

4137.png

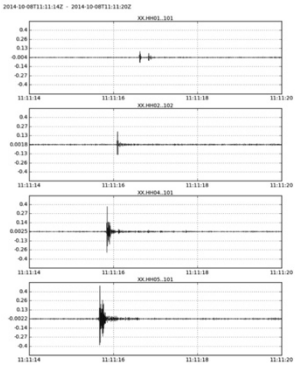

4275.png

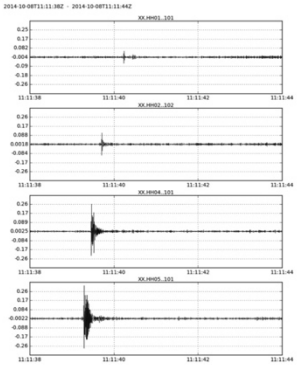

4299.png

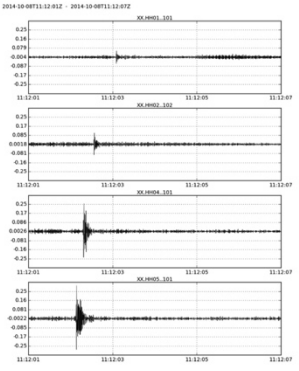

4322.png

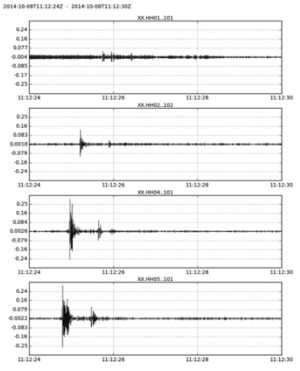

4345.png

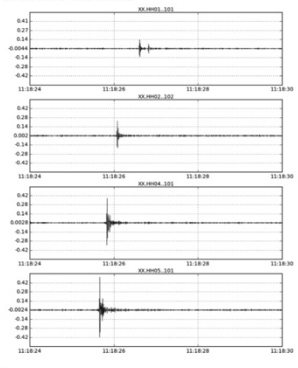

4705.png

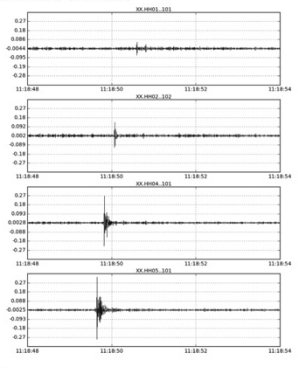

4729.png

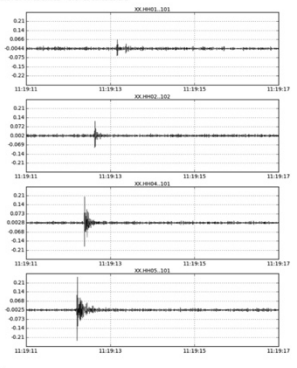

4752.png

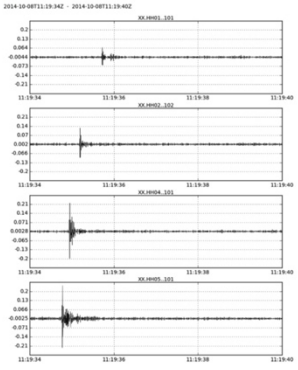

4775.png

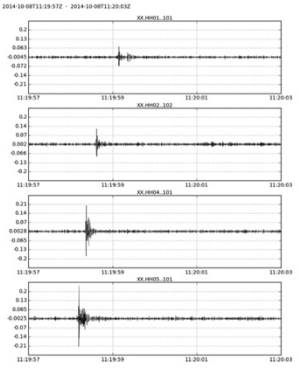

4798.png

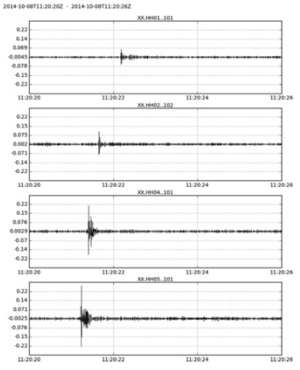

4821.png

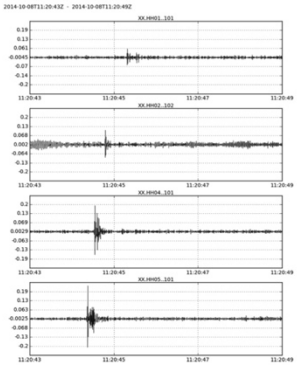

4844.png

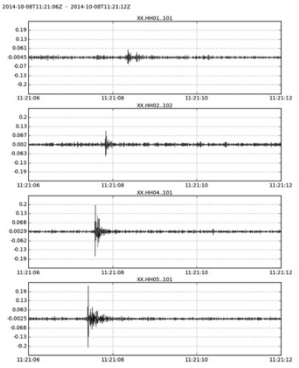

4867.png

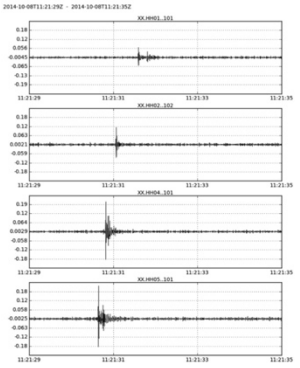

4890.png

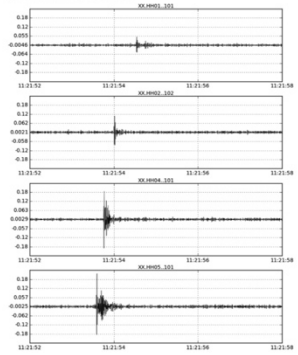

4913.png

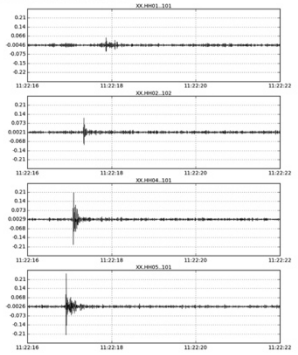

4937.png

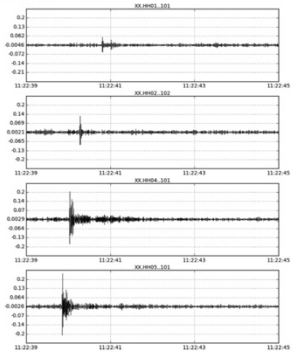

4960.png

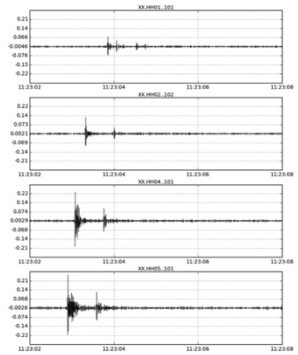

4983.png

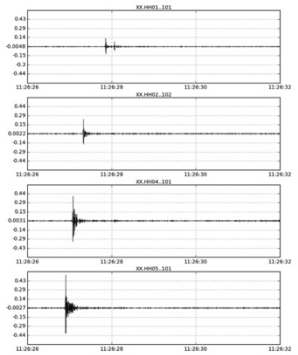

5187.png

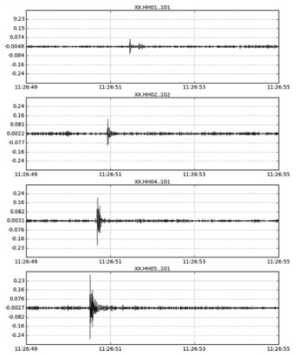

5210.png

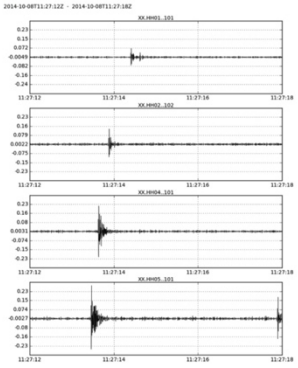

5233.png

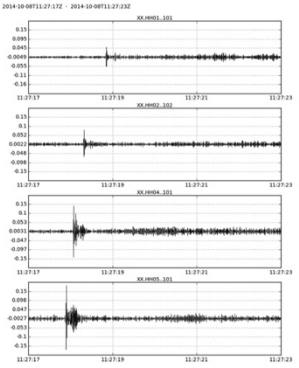

5238.png

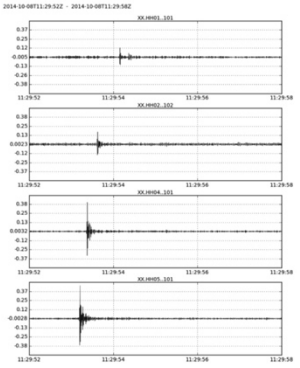

5393.png

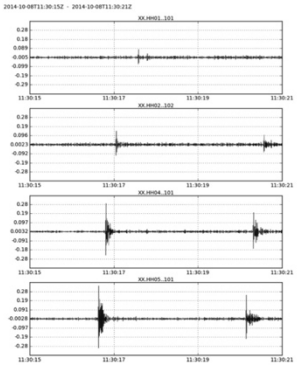

5416.png

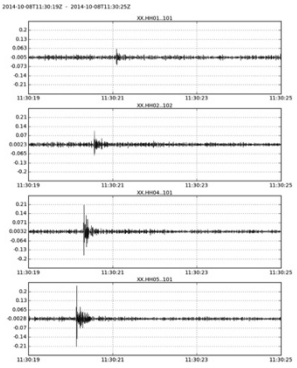

5420.png

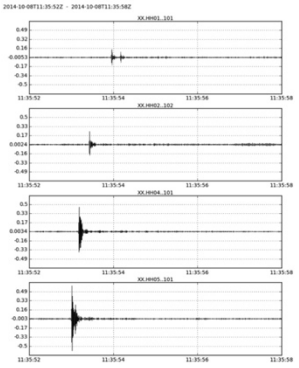

5753.png

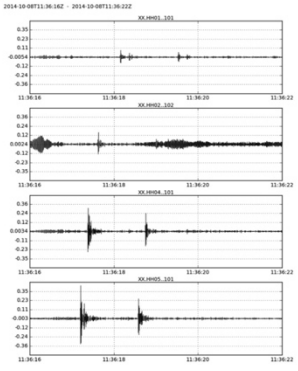

5777.png

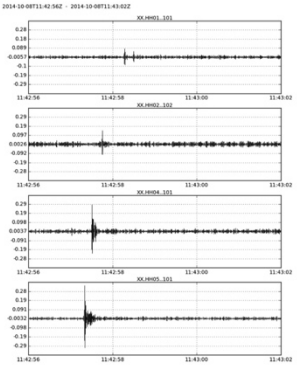

6177.png

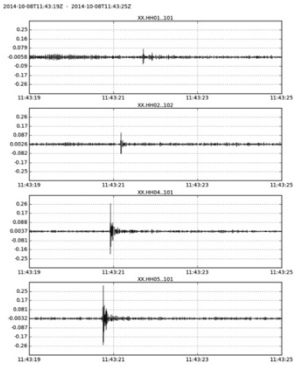

6200.png

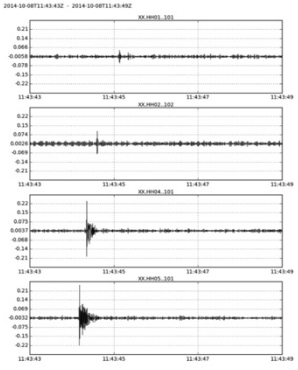

6224.png

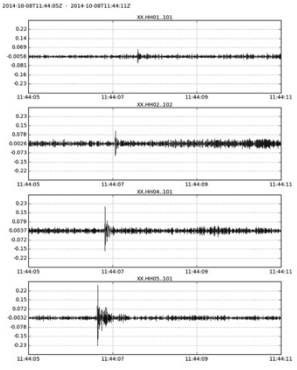

6246.png

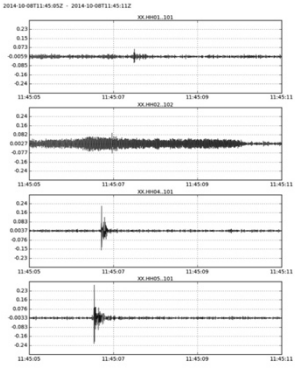

6306.png

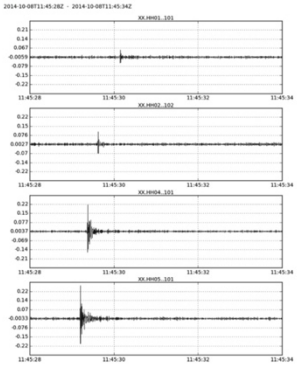

6329.png

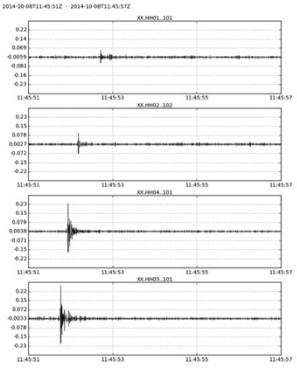

6352.png

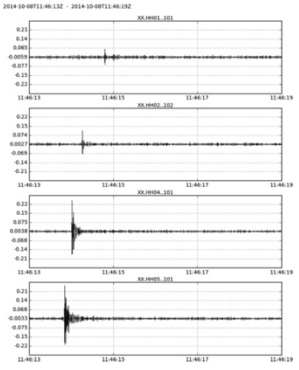

6374.png

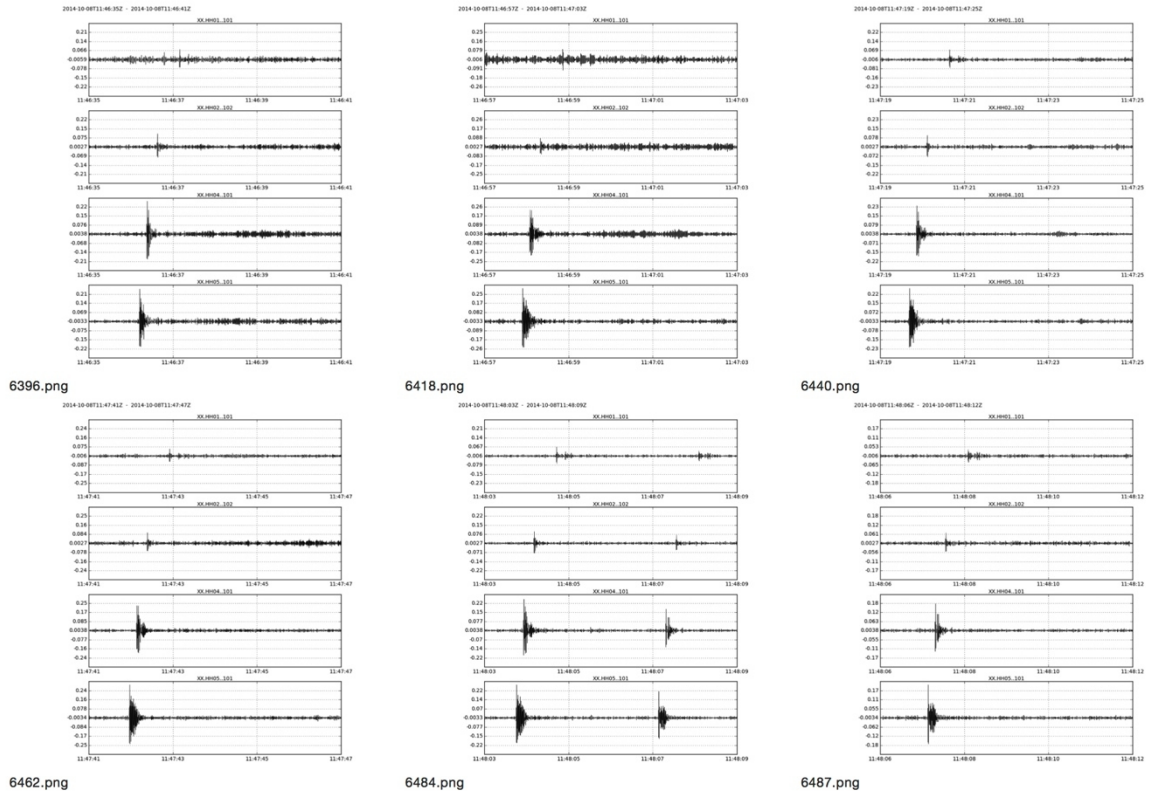

Figure 10. The above waveform plots are windowed for each triggered event during the experiment. In some cases the hammer bounced after the initial shot resulting in a second event. Amplitude is in Pa.

APPENDIX B: SPECTROGRAM PLOTS

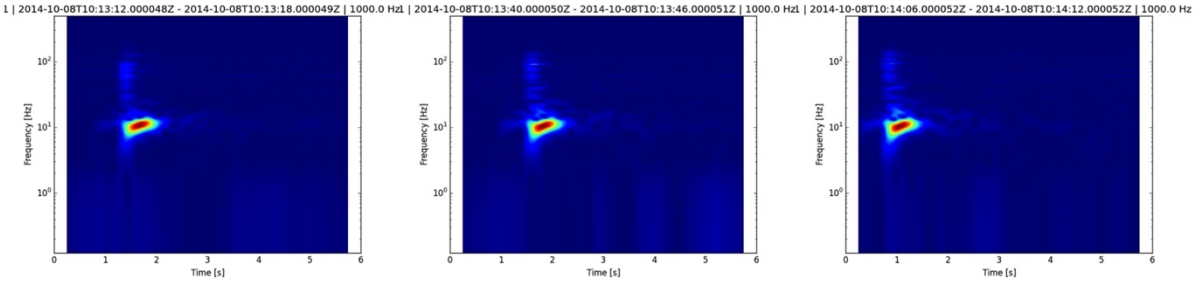

793_spec.png 821_spec.png 847_spec.png

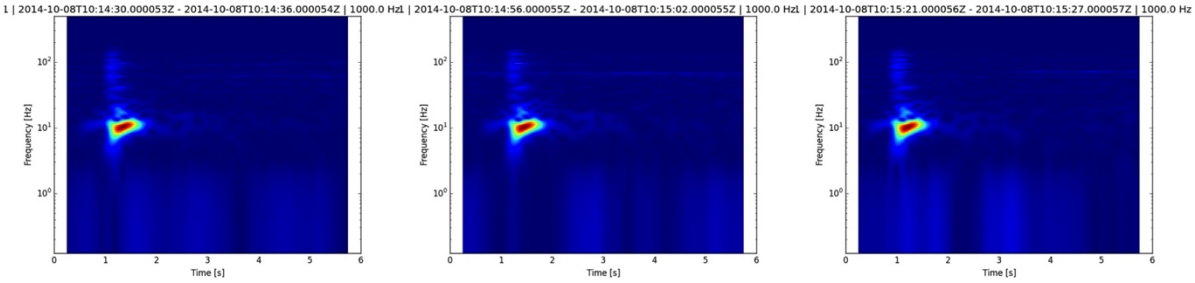

871_spec.png 897_spec.png 922_spec.png

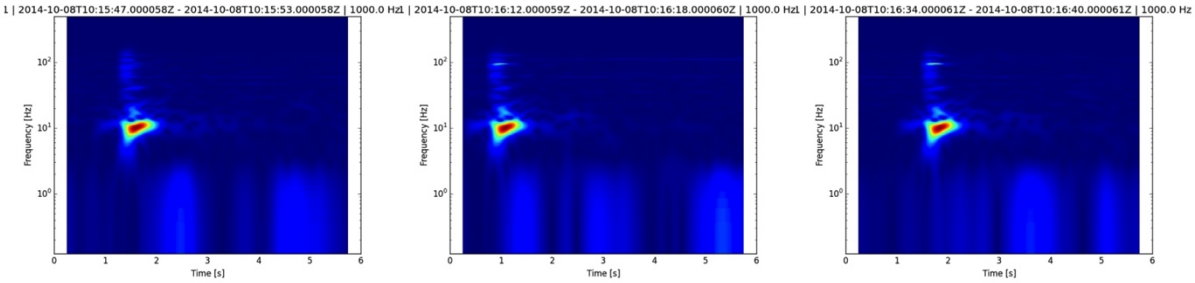

948_spec.png 973_spec.png 995_spec.png

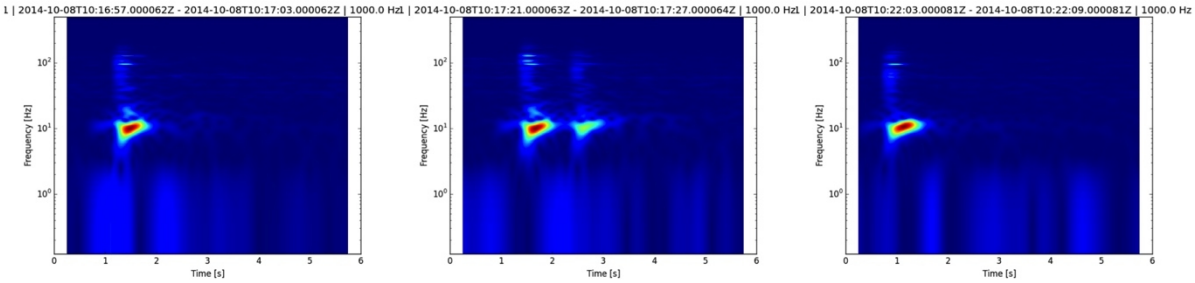

1018_spec.png 1042_spec.png 1324_spec.png

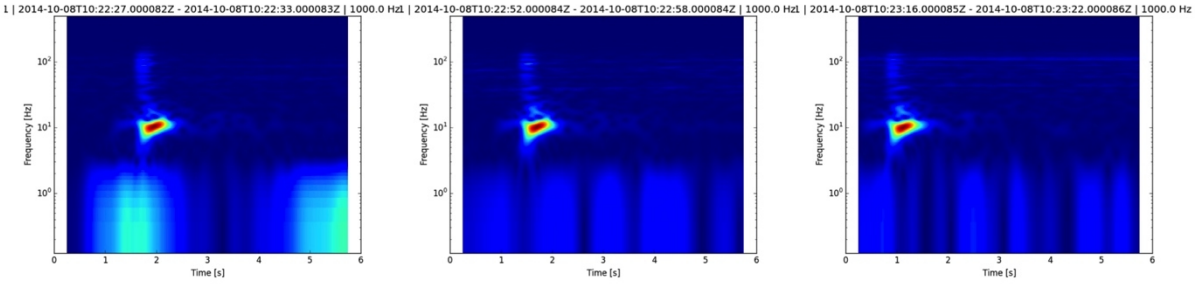

1348_spec.png 1373_spec.png 1397_spec.png

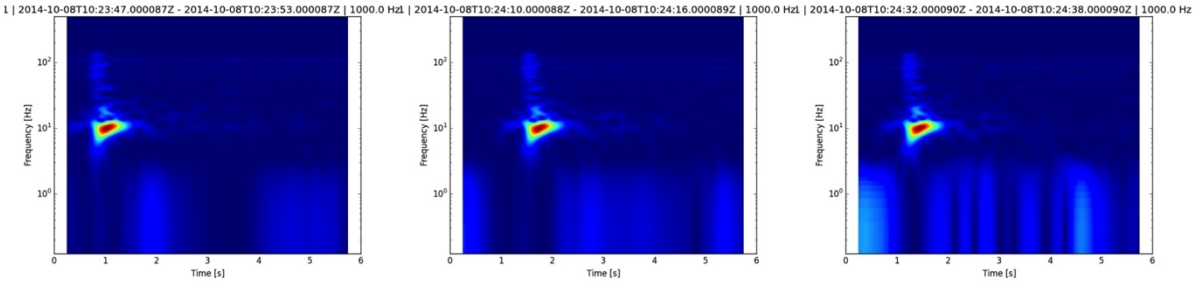

1428_spec.png 1451_spec.png 1473_spec.png

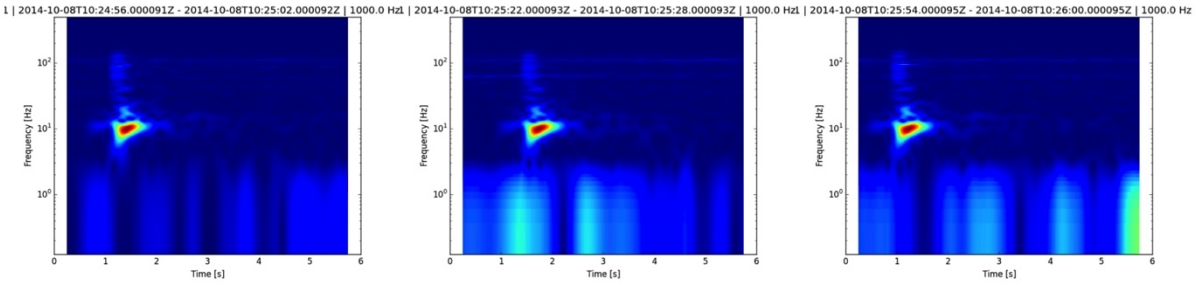

1497_spec.png 1523_spec.png 1555_spec.png

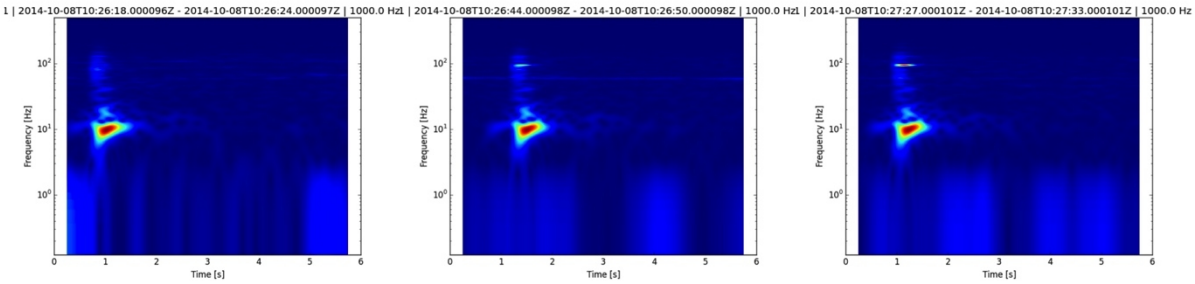

1579_spec.png 1605_spec.png 1648_spec.png

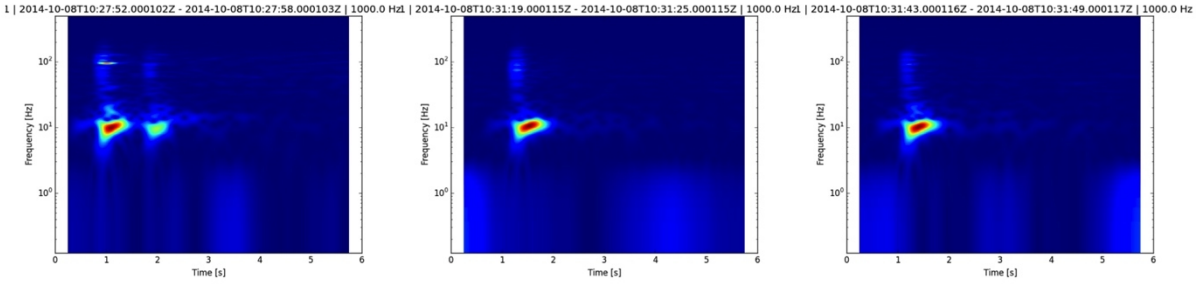

1673_spec.png 1880_spec.png 1904_spec.png

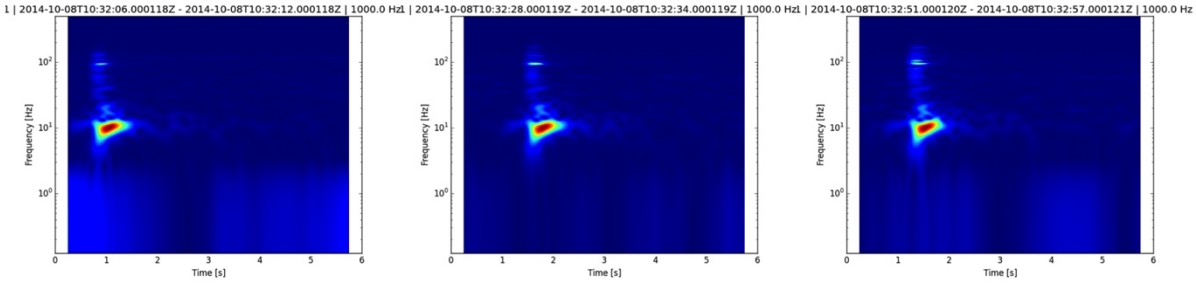

1927_spec.png 1949_spec.png 1972_spec.png

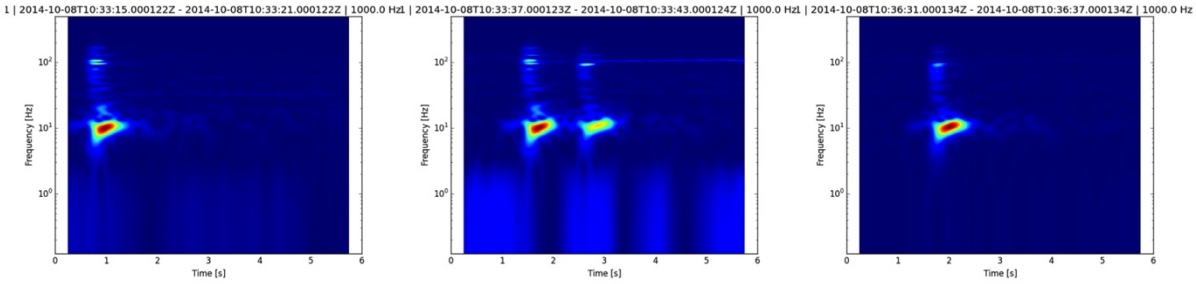

1996_spec.png 2018_spec.png 2192_spec.png

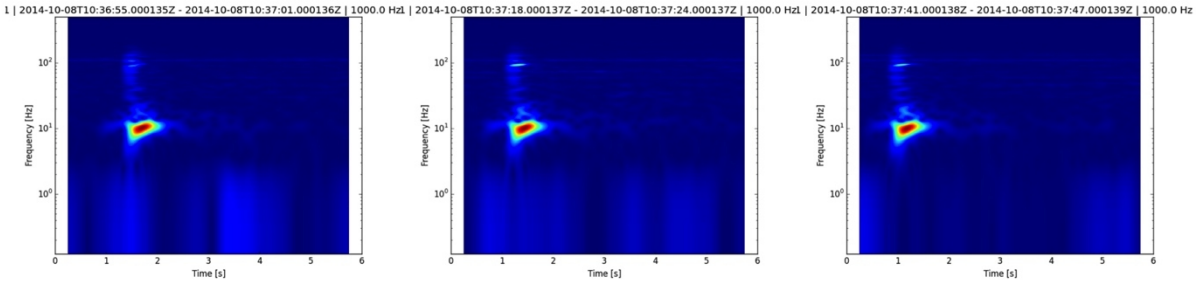

2216_spec.png 2239_spec.png 2262_spec.png

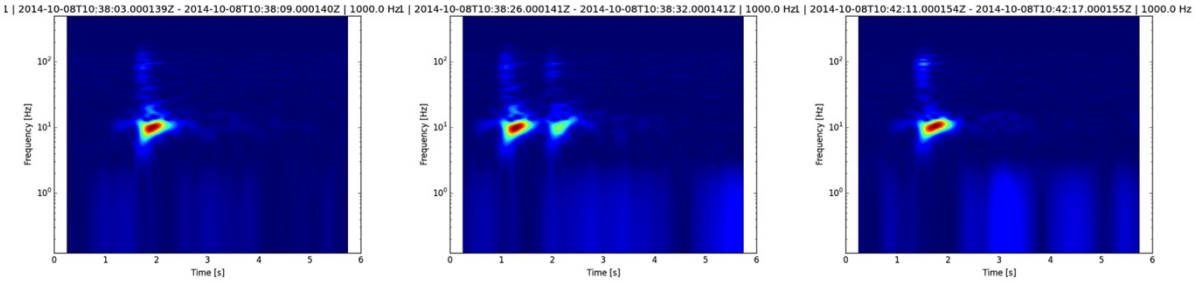

2284_spec.png 2307_spec.png 2532_spec.png

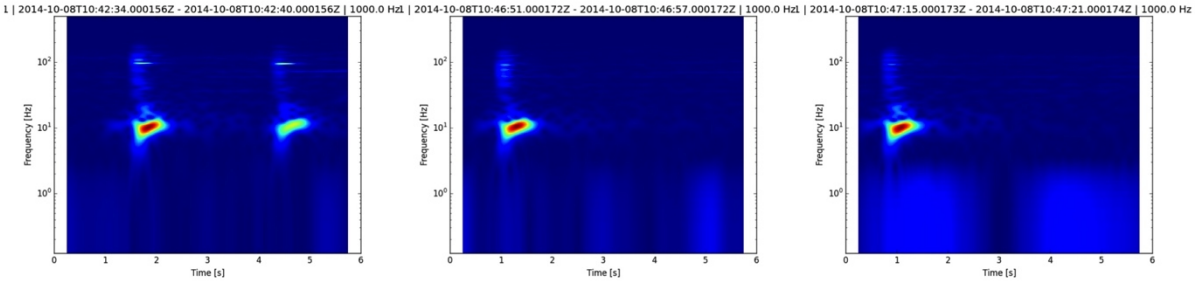

2555_spec.png 2812_spec.png 2836_spec.png

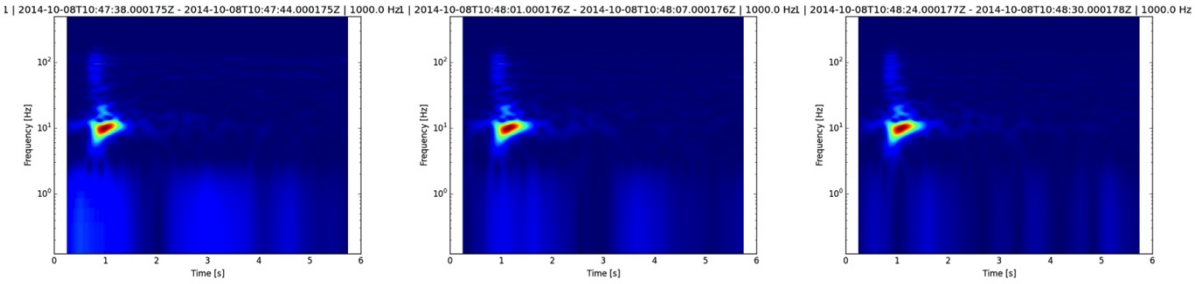

2859_spec.png 2882_spec.png 2905_spec.png

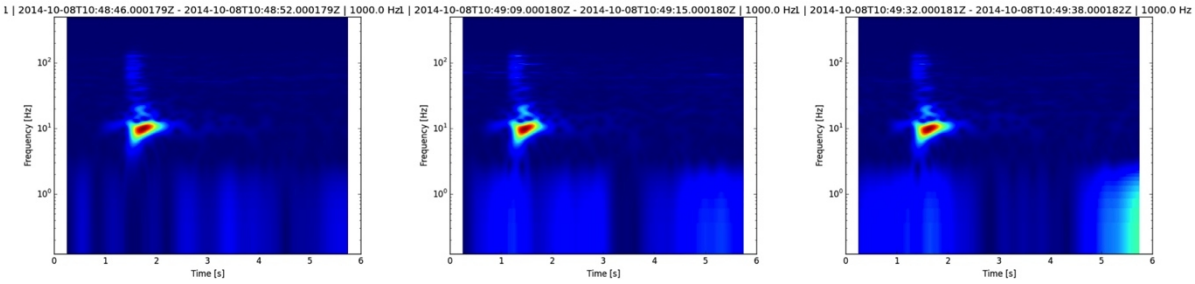

2927_spec.png 2950_spec.png 2973_spec.png

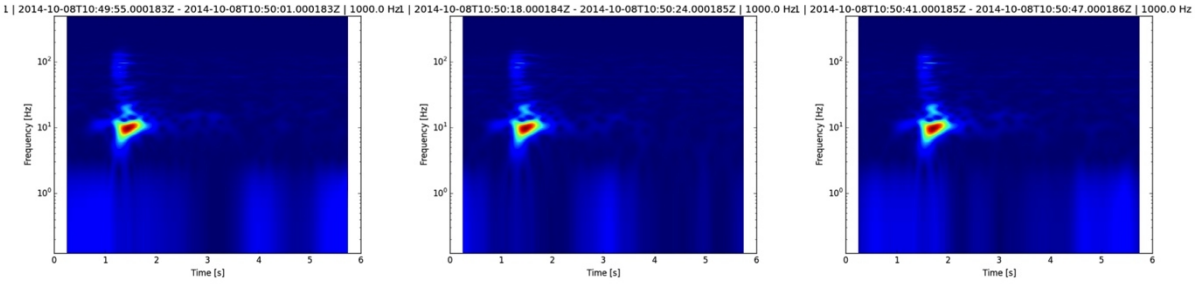

2996_spec.png 3019_spec.png 3042_spec.png

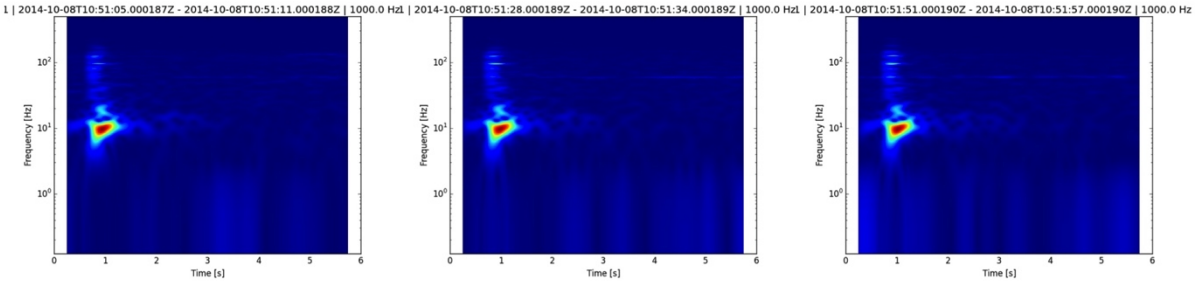

3066_spec.png 3089_spec.png 3112_spec.png

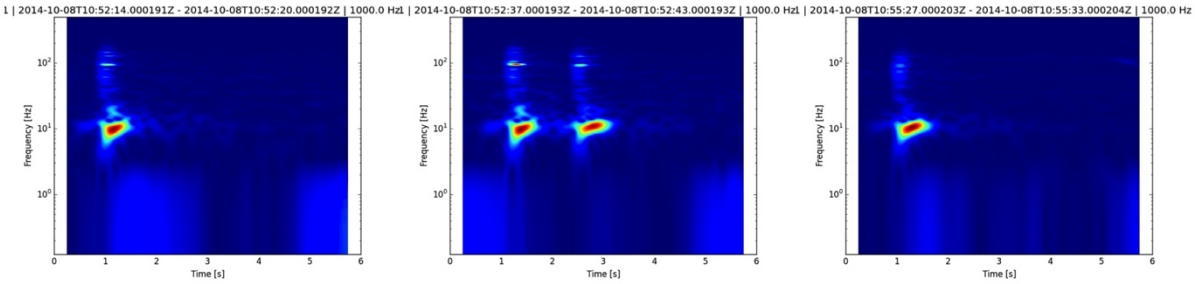

3135_spec.png 3158_spec.png 3328_spec.png

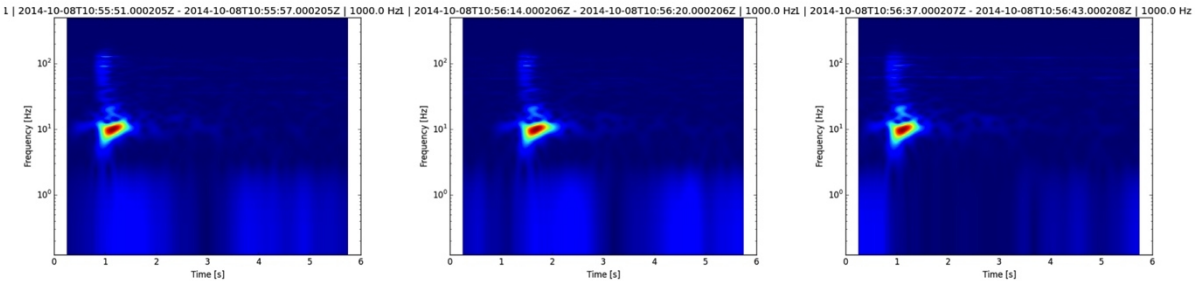

3352_spec.png 3375_spec.png 3398_spec.png

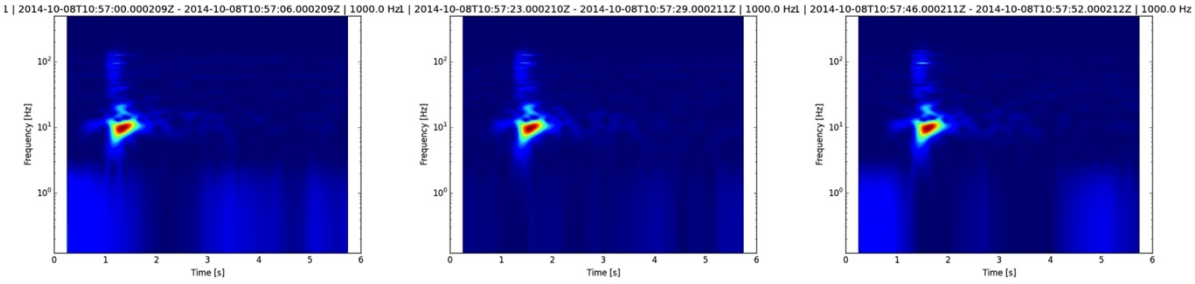

3421_spec.png 3444_spec.png 3467_spec.png

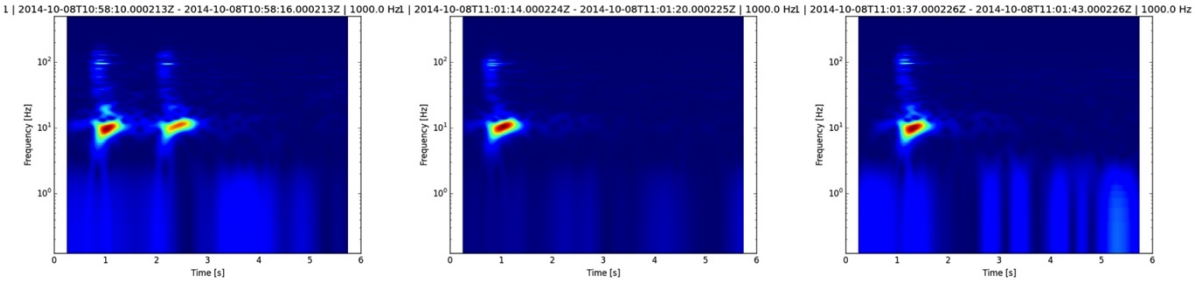

3491_spec.png 3675_spec.png 3698_spec.png

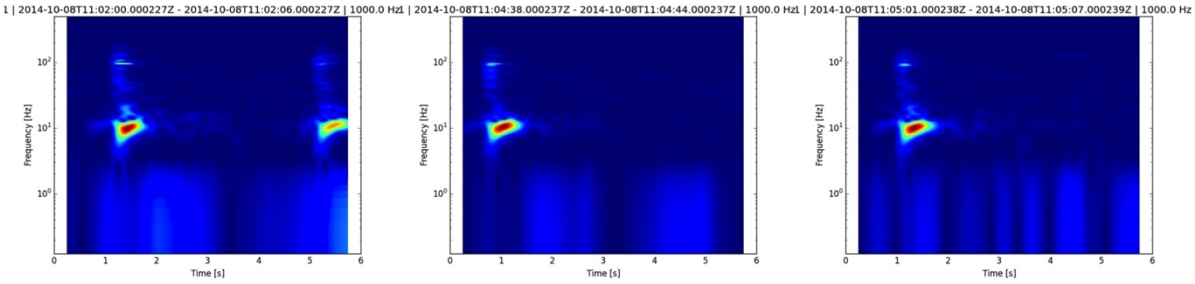

3721_spec.png 3879_spec.png 3902_spec.png

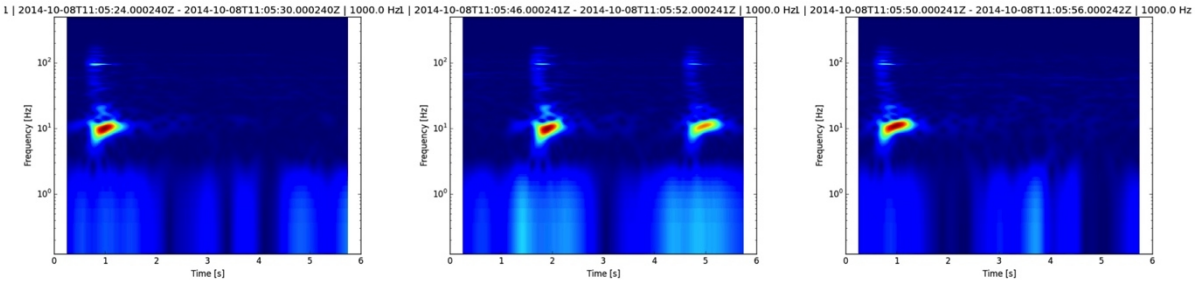

3925_spec.png 3947_spec.png 3951_spec.png

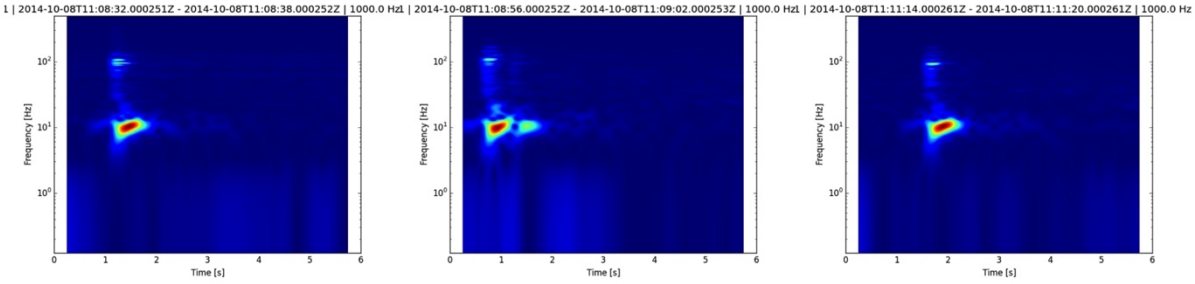

4113_spec.png 4137_spec.png 4275_spec.png

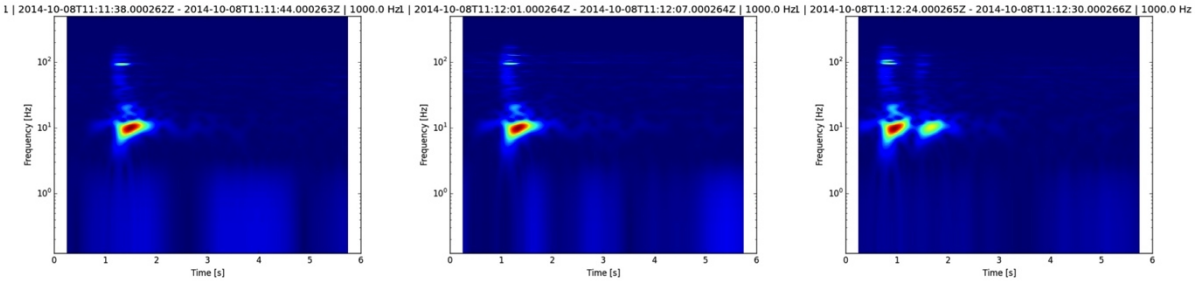

4299_spec.png 4322_spec.png 4345_spec.png

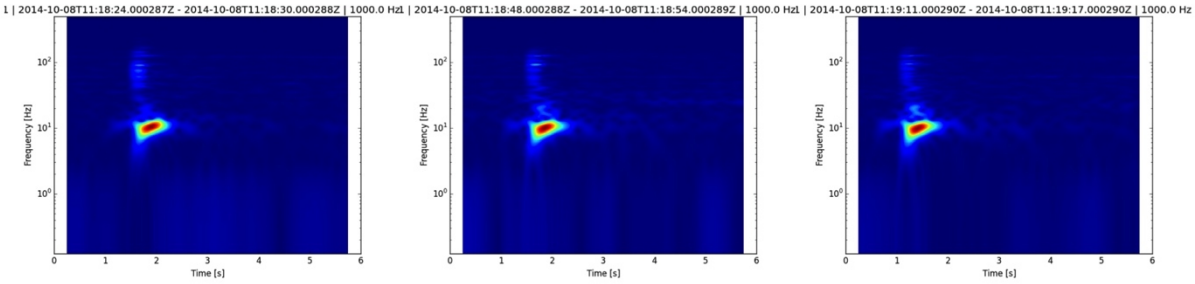

4705_spec.png 4729_spec.png 4752_spec.png

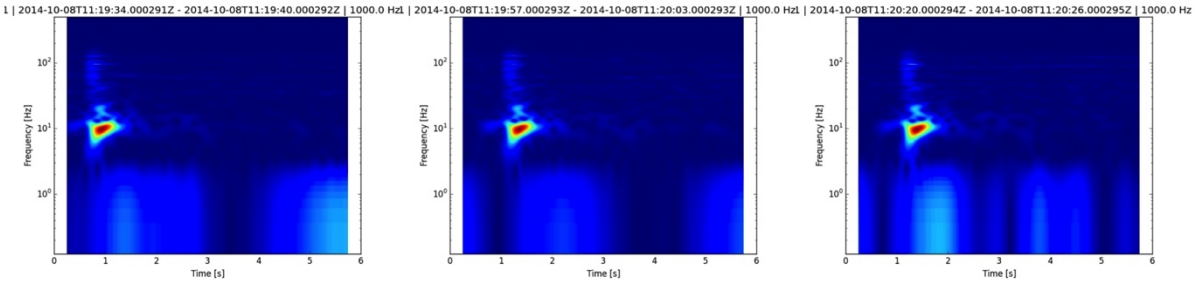

4775_spec.png 4798_spec.png 4821_spec.png

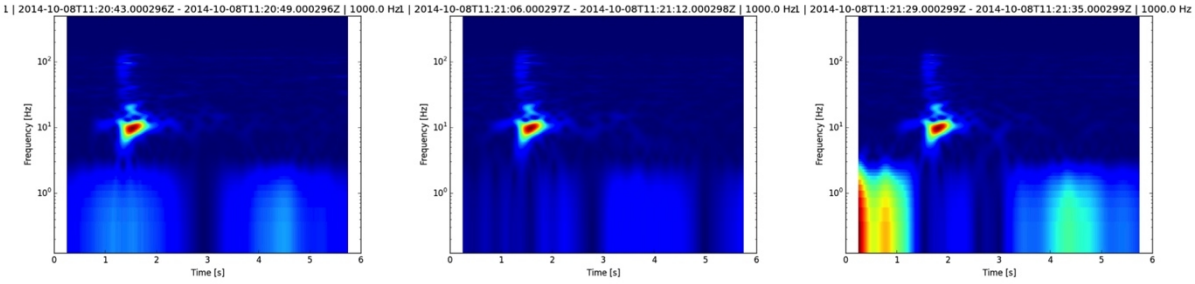

4844_spec.png 4867_spec.png 4890_spec.png

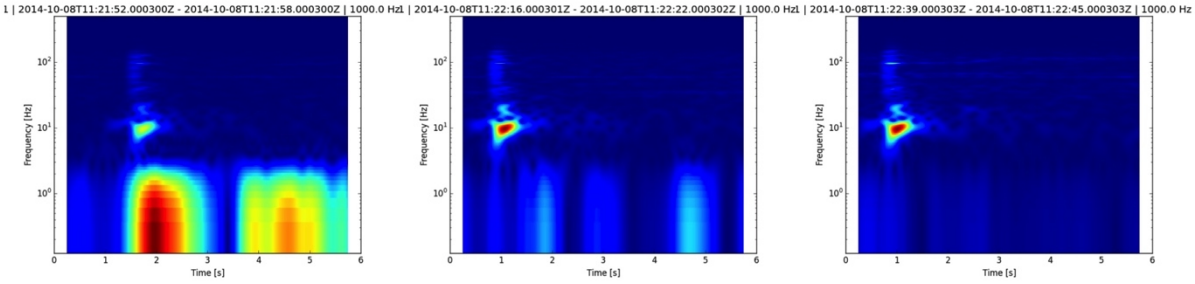

4913_spec.png 4937_spec.png 4960_spec.png

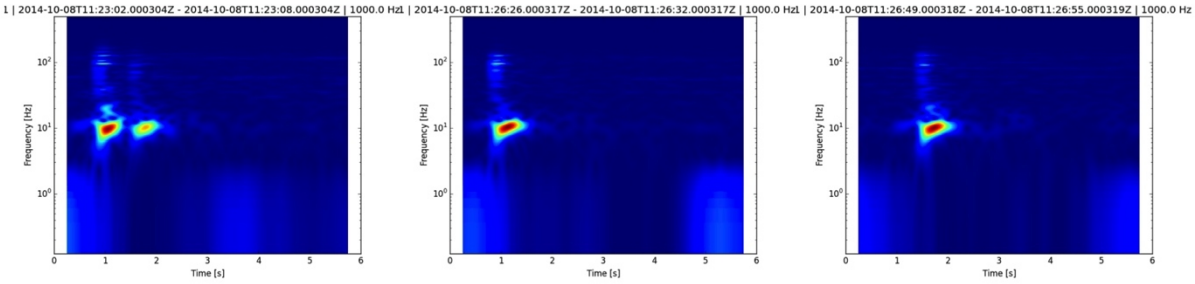

4983_spec.png 5187_spec.png 5210_spec.png

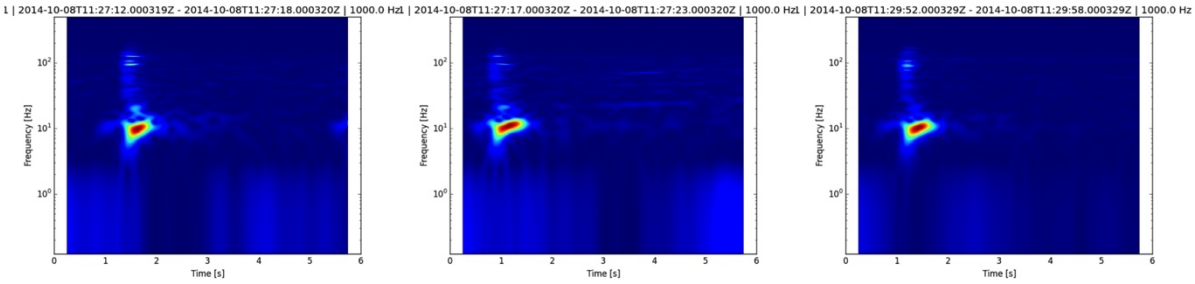

5233_spec.png 5238_spec.png 5393_spec.png

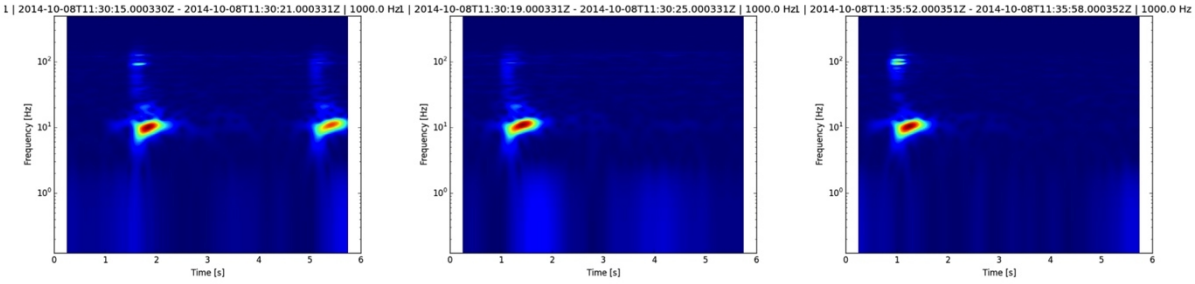

5416_spec.png 5420_spec.png 5753_spec.png

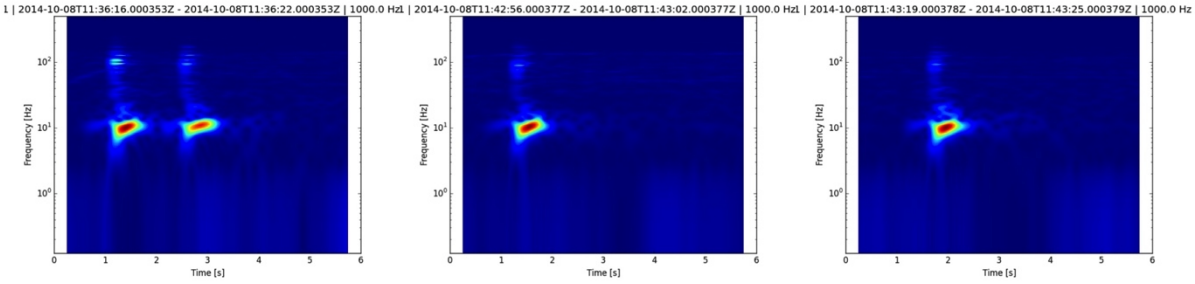

5777_spec.png 6177_spec.png 6200_spec.png

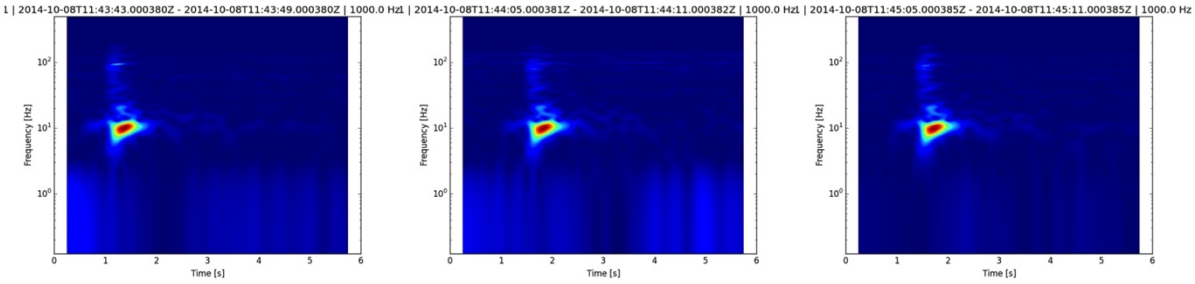

6224_spec.png 6246_spec.png 6306_spec.png

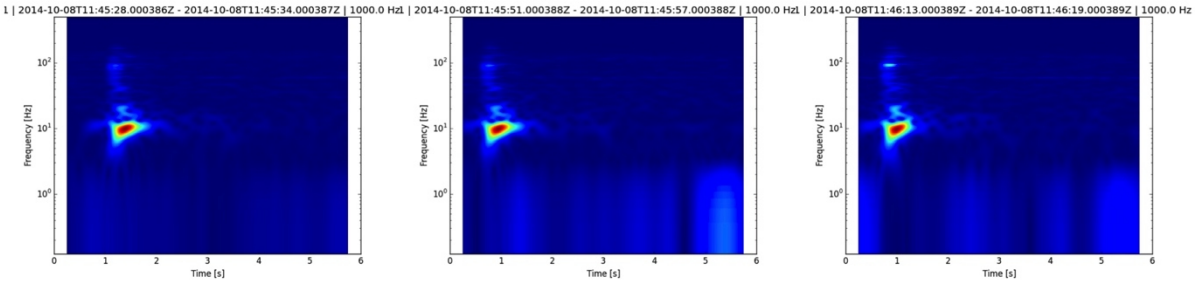

6329_spec.png 6352_spec.png 6374_spec.png

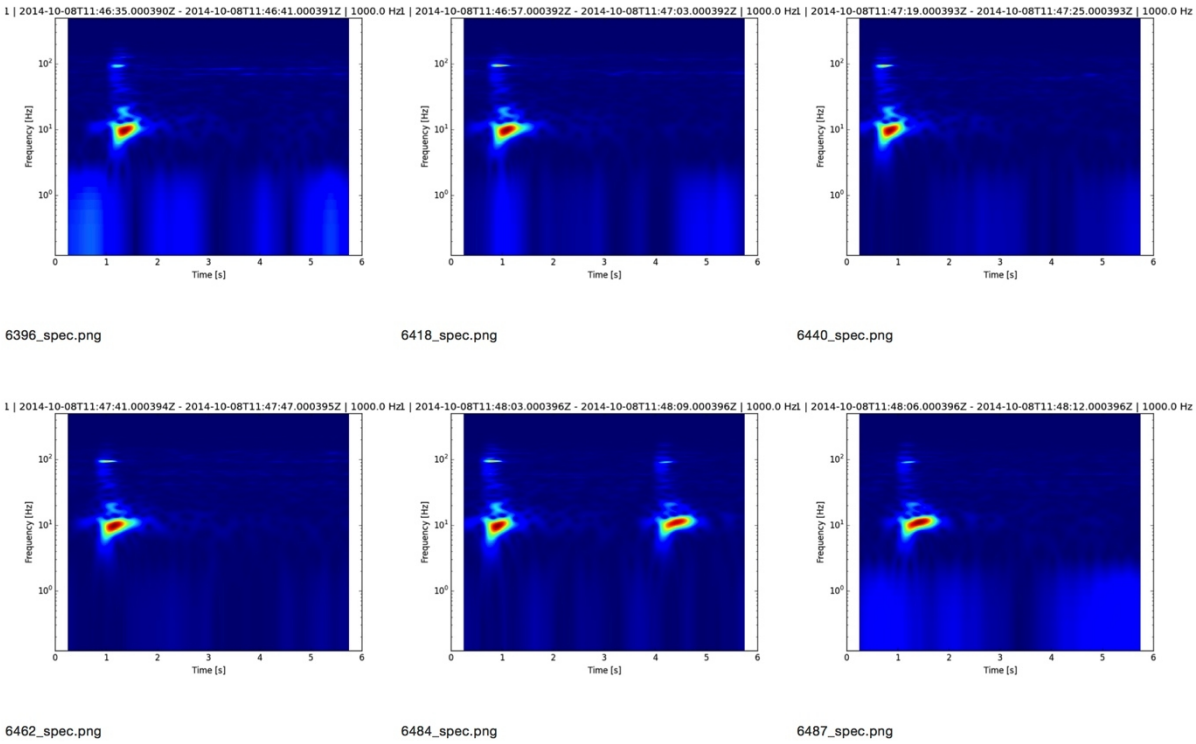

Figure 11. The above spectrograms are windowed for each triggered event during the experiment and are plotted as log frequency vs. time in seconds. The “shots” are very similar throughout the experiment. In some cases the hammer bounced after the initial shot resulting in a second event.

APPENDIX C: TRIGGER TABLE

Trigger # (seconds)	Time Lag 5 (s)	Time Lag 4 (s)	Time Lag 2 (s)	Time Lag 1 (s)	Latitude	Longitude
793	0	0.174	0.42	0.95	36.2362258873	-115.111591215
821	0	0.172	0.42	0.948	36.2362914237	-115.111560394
847	0	0.172	0.42	0.95	36.2363006648	-115.111561894
871	0	0.172	0.42	0.95	36.2363006648	-115.111561894
897	0	0.172	0.42	0.95	36.2363006648	-115.111561894
922	0	0.172	0.42	0.948	36.2362914237	-115.111560394
948	0	0.172	0.42	0.95	36.2363006648	-115.111561894
973	0	0.174	0.422	0.95	36.2362481056	-115.111587577
995	0	0.174	0.422	0.95	36.2362481056	-115.111587577
1018	0	0.172	0.42	0.95	36.2363006648	-115.111561894
1042	0	0.172	0.42	0.95	36.2363006648	-115.111561894
1324	0	0.172	0.42	0.95	36.2363006648	-115.111561894
1348	0	0.172	0.42	0.95	36.2363006648	-115.111561894
1373	0	0.174	0.422	0.95	36.2362481056	-115.111587577
1397	0	0.172	0.42	0.95	36.2363006648	-115.111561894
1428	0	0.174	0.422	0.952	36.2362580304	-115.111588859
1451	0	0.174	0.422	0.952	36.2362580304	-115.111588859
1473	0	0.174	0.422	0.952	36.2362580304	-115.111588859
1497	0	0.172	0.42	0.95	36.2363006648	-115.111561894
1523	0	0.172	0.42	0.952	36.2363094108	-115.111563562
1555	0	0.174	0.422	0.952	36.2362580304	-115.111588859
1579	0	0.174	0.422	0.952	36.2362580304	-115.111588859
1605	0	0.174	0.422	0.952	36.2362580304	-115.111588859
1648	0	0.172	0.422	0.952	36.2363306941	-115.111560248
1673	0	0.172	0.422	0.952	36.2363306941	-115.111560248
1880	0	0.172	0.42	0.95	36.2363006648	-115.111561894
1904	0	0.174	0.422	0.95	36.2362481056	-115.111587577
1927	0	0.172	0.42	0.95	36.2363006648	-115.111561894
1949	0	0.174	0.422	0.95	36.2362481056	-115.111587577
1972	0	0.174	0.42	0.95	36.2362258873	-115.111591215
1996	0	0.174	0.422	0.95	36.2362481056	-115.111587577
2018	0	0.172	0.422	0.95	36.2363222075	-115.111558523
2192	0	0.174	0.422	0.95	36.2362481056	-115.111587577
2216	0	0.174	0.422	0.95	36.2362481056	-115.111587577
2239	0	0.172	0.422	0.95	36.2363222075	-115.111558523
2262	0	0.172	0.42	0.95	36.2363006648	-115.111561894
2284	0	0.172	0.42	0.95	36.2363006648	-115.111561894
2307	0	0.172	0.422	0.95	36.2363222075	-115.111558523
2532	0	0.174	0.422	0.952	36.2362580304	-115.111588859
2555	0	0.172	0.422	0.95	36.2363222075	-115.111558523
2812	0	0.172	0.42	0.95	36.2363006648	-115.111561894
2836	0	0.174	0.422	0.952	36.2362580304	-115.111588859
2859	0	0.174	0.422	0.95	36.2362481056	-115.111587577
2882	0	0.172	0.422	0.95	36.2363222075	-115.111558523
2905	0	0.172	0.42	0.95	36.2363006648	-115.111561894
2927	0	0.172	0.42	0.95	36.2363006648	-115.111561894

2950	0	0.174	0.422	0.952	36.2362580304	-115.111588859
2973	0	0.172	0.422	0.952	36.2363306941	-115.111560248
2996	0	0.172	0.42	0.952	36.2363094108	-115.111563562
3019	0	0.174	0.422	0.952	36.2362580304	-115.111588859
3042	0	0.172	0.42	0.95	36.2363006648	-115.111561894
3066	0	0.172	0.422	0.952	36.2363306941	-115.111560248
3089	0	0.172	0.422	0.952	36.2363306941	-115.111560248
3112	0	0.172	0.422	0.952	36.2363306941	-115.111560248
3135	0	0.172	0.422	0.952	36.2363306941	-115.111560248
3158	0	0.174	0.424	0.952	36.2362804083	-115.111585063
3328	0	0.174	0.422	0.952	36.2362580304	-115.111588859
3352	0	0.174	0.422	0.952	36.2362580304	-115.111588859
3375	0	0.172	0.422	0.95	36.2363222075	-115.111558523
3398	0	0.172	0.422	-0.546	36.2363222075	-115.111558523
3421	0	0.174	0.422	0.952	36.2362580304	-115.111588859
3444	0	0.172	0.422	0.952	36.2363306941	-115.111560248
3467	0	0.172	0.422	0.952	36.2363306941	-115.111560248
3491	0	0.172	0.422	0.952	36.2363306941	-115.111560248
3675	0	0.172	0.422	0.952	36.2363306941	-115.111560248
3698	0	0.174	0.424	0.954	36.2362894968	-115.111586608
3721	0	0.174	0.424	0.954	36.2362894968	-115.111586608
3879	0	0.174	0.424	0.954	36.2362894968	-115.111586608
3902	0	0.172	0.422	0.952	36.2363306941	-115.111560248
3925	0	0.172	0.424	0.952	36.2363523276	-115.111556758
3947	0	0.172	0.422	0.952	36.2363306941	-115.111560248
3951	0	0.172	0.422	1.162	36.2363306941	-115.111560248
4113	0	0.172	0.422	0.95	36.2363222075	-115.111558523
4137	0	0.172	0.422	0.952	36.2363306941	-115.111560248
4275	0	0.172	0.422	0.95	36.2363222075	-115.111558523
4299	0	0.172	0.42	0.95	36.2363006648	-115.111561894
4322	0	0.172	0.42	0.95	36.2363006648	-115.111561894
4345	0	0.172	0.42	0.95	36.2363006648	-115.111561894
4705	0	0.172	0.42	0.948	36.2362914237	-115.111560394
4729	0	0.172	0.42	0.946	36.2362816578	-115.111559072
4752	0	0.172	0.42	0.948	36.2362914237	-115.111560394
4775	0	0.172	0.418	0.946	36.2362599616	-115.111562372
4798	0	0.172	0.418	0.946	36.2362599616	-115.111562372
4821	0	0.172	0.418	0.946	36.2362599616	-115.111562372
4844	0	0.172	0.418	0.946	36.2362599616	-115.111562372
4867	0	0.172	0.42	0.946	36.2362816578	-115.111559072
4890	0	0.172	0.418	0.946	36.2362599616	-115.111562372
4913	0	0.172	0.418	0.946	36.2362599616	-115.111562372
4937	0	0.172	0.418	0.946	36.2362599616	-115.111562372
4960	0	0.174	0.42	0.948	36.2362150676	-115.111590214
4983	0	0.172	0.418	0.946	36.2362599616	-115.111562372
5187	0	0.172	0.42	0.948	36.2362914237	-115.111560394
5210	0	0.172	0.42	0.948	36.2362914237	-115.111560394
5233	0	0.172	0.42	0.948	36.2362914237	-115.111560394
5238	0	0.174	0.42	0.948	36.2362150676	-115.111590214
5393	0	0.172	0.42	0.948	36.2362914237	-115.111560394

5416	0	0.172	0.42	0.948	36.2362914237	-115.111560394
5420	0	0.172	0.42	0.948	36.2362914237	-115.111560394
5753	0	0.174	0.42	0.95	36.2362258873	-115.111591215
5777	0	0.172	0.42	0.948	36.2362914237	-115.111560394
6177	0	0.174	0.42	0.95	36.2362258873	-115.111591215
6200	0	0.174	0.42	0.95	36.2362258873	-115.111591215
6224	0	0.174	0.422	0.952	36.2362580304	-115.111588859
6246	0	0.174	0.42	0.952	36.2362360996	-115.111592431
6306	0	0.174	0.42	0.95	36.2362258873	-115.111591215
6329	0	0.172	0.42	0.95	36.2363006648	-115.111561894
6352	0	0.174	0.422	0.952	36.2362580304	-115.111588859
6374	0	0.172	0.42	0.95	36.2363006648	-115.111561894
6396	0	0.174	0.422	0.95	36.2362481056	-115.111587577
6418	0	0.174	0.42	0.95	36.2362258873	-115.111591215
6440	0	0.174	0.422	0.952	36.2362580304	-115.111588859
6462	0	0.172	0.42	0.95	36.2363006648	-115.111561894
6484	0	0.174	0.42	0.952	36.2362360996	-115.111592431
6487	0	0.172	0.42	0.95	36.2363006648	-115.111561894

Table 2. Table showing all of the auto-detected event triggers for the two-hour period during the experiment. The first column corresponds to the trigger time in seconds from 10:00:00 UTC. Columns 2 – 5 show the time lags from each station (1,2,4,5) used during the source inversion. Station 5 was used as the zero time from which the other time lags are relative to. The final two columns show the latitude and longitude from the source inversion.

DISTRIBUTION

1 HH Seismic
Attn: John Hampshire
24325 Crenshaw Ave #146
Torrance, CA 90503-5349

1	MS0404	Kyle R. Jones	5752
1	MS0404	Neill Symons	5752
1	MS0406	Steve Vigil	5751 (electronic copy)
1	MS0750	Rob Abbott	6913 (electronic copy)
1	MS1141	Bob Huelskamp	5750

1	MS0899	Technical Library	9536 (electronic copy)


Sandia National Laboratories